Article

Targeting the Hemopexin-like Domain of Latent Matrix Metalloproteinase-9 (proMMP-9) with a Small Molecule Inhibitor Prevents the Formation of Focal Adhesion Junctions

Vincent M. Alford, Anushree Kamath, Xiaodong Ren, kunal kumar, Qianwen Gan, Monaf Awwa, Michael Tong, Markus A Seeliger, Jian Cao, Iwao Ojima, and Nicole S Sampson

ACS Chem. Biol., **Just Accepted Manuscript** • DOI: 10.1021/acschembio.7b00758 • Publication Date (Web): 25 Sep 2017

Targeting the Hemopexin-like Domain of Latent Matrix Metalloproteinase-9 (proMMP-9) with a Small Molecule Inhibitor Prevents the Formation of Focal Adhesion Junctions

Short title: PEX-9 Inhibitors Prevent Formation of Focal Adhesion Junctions

Vincent M. Alford,[1,3] Anushree Kamath,[2] Xiaodong Ren,[2] Kunal Kumar,[2] Qianwen Gan,[2] Monaf Awwa,[2] Michael Tong,[1] Markus A. Seeliger,[1,4] Jian Cao,[3] Iwao Ojima,[2,4] Nicole S. Sampson [2,4*]

[1]*Department of Molecular and Cellular Pharmacology, Stony Brook University, Stony Brook, NY, USA*

[2]*Department of Chemistry, Stony Brook University, Stony Brook, NY, USA*

[3]*Department of Medicine, Stony Brook University, Stony Brook, NY, USA*

[4]*Institute of Chemical Biology & Drug Discovery, Stony Brook, NY, USA*

*Corresponding author. Tel. & Fax: (631) 632-7952 | (631) 632-5731 Email: nicole.sampson@stonybrook.edu

ABSTRACT: A lack of target specificity has greatly hindered the success of inhibitor development against matrix metalloproteinases (MMPs) for the treatment of various cancers. The MMP catalytic domains are highly conserved, whereas the hemopexin-like domain of MMPs are unique to each family member. The hemopexin-like domain of MMP-9 enhances cancer cell migration through self-interaction and hetero-interactions with cell surface proteins including CD44 and $\alpha4\beta1$ integrin. These interactions activate EGFR-MAP kinase dependent signaling that leads to cell migration. In this work, we generated a library of compounds, based on hit molecule, *N*-[4-(difluoromethoxy)phenyl]-2-[(4-oxo-6-propyl-1*H*-pyrimidin-2-yl)sulfanyl]-acetamide, that target the hemopexin-like domain of MMP-9. We identify *N*-(4-fluorophenyl)-4-(4-oxo-3,4,5,6,7,8-hexahydroquinazolin-2-ylthio)butanamide, **3c**, as a potent lead (K_d = 320 nM) that is specific for binding to proMMP-9 hemopexin-like domain. We demonstrate that **3c** disruption of MMP-9 homodimerization prevents association of proMMP-9 with both α4β1 integrin and CD44 and results in dissociation of EGFR. This disruption results in decreased phosphorylation of Src and its downstream target proteins focal adhesion kinase (FAK) and paxillin (PAX), which are implicated in promoting tumor cell growth, migration, and invasion. Using a chicken chorioallantoic membrane *in vivo* assay, we demonstrate that 500 nM **3c** blocks cancer cell invasion of the basement membrane and reduces angiogenesis. In conclusion, we present a mechanism of action for **3c** whereby targeting the hemopexin domain results in decreased cancer cell migration through simultaneous disruption of $\alpha4\beta1$ integrin and EGFR signaling pathways, thereby preventing signaling bypass. Targeting through the hemopexin-like domain is a powerful approach to anti-metastatic drug development.

Keywords: MMP-9; hemopexin domain; PEX-9 inhibitors; focal adhesions; metastasis.

INTRODUCTION

Metastasis accounts for 90% of all human cancer related deaths yet we lack adequate drugs to target this biological process often associated with aggressive cancers.[1] Accumulating evidence suggests an important role for matrix metalloproteinases (MMPs) in promoting cancer progression whereby they modify their surrounding environment to promote the growth and spread of tumor cells.[2-5] Although MMPs represent the most prominent family of proteinases associated with tumorigenesis, drugs designed to inhibit their proteolytic activities largely failed in clinical trials due to issues with selectivity for individual MMPs.[6] The highly conserved catalytic domain within this family of zymogens required a paradigm shift to the development of novel MMP inhibitors (MMPIs) targeting less conserved, non-catalytic functional domain(s) of the proteases to increase target specificity and selectivity.[7]

The biological functions of MMPs extend beyond just their proteolytic function, and include induction of complex signaling cascades.[8-10] Homodimerization of secreted proMMP-9 hemopexin domains is sufficient to induce cancer cell migration independent of proteolytic activity.[11] Using an shRNA approach the mechanism behind this phenotype was dissected and found to be dependent on an interaction between MMP-9 and CD44 at the cell surface. This interaction required an intact MMP-9 hemopexin domain (PEX-9). Interaction between CD44 and PEX-9 results in increased epidermal growth factor receptor (EGFR) phosphorylation and subsequent activation of mitogen-activated protein kinase (MAPK)/extracellular signal–regulated kinases (ERK) signaling, thereby enhancing the migratory capacity of proMMP-9 expressing cancer cells.[12] Signaling was lost upon deletion or swapping of PEX-9 with the PEX domain of its closest homolog MMP-2.

The X-ray crystal structure of the PEX domain of MMP-9 has been solved. PEX-9 forms a propeller-like structure composed of four blades, which converge and are linked between blades I and IV through disulfide bonds.[13] Each blade of the PEX domain is composed of a

single α-helix and four anti-parallel β-strands. They form a scaffold for substrate recognition and docking[14]

Published reports have shown that PEX-9 can interact with different integrin subunits to promote enhanced cancer cell migration, invasion, and survival in various cancer cell types.[15-20] Of particular interest to our study was a recent finding that peptide sequence FPGVPLDTHDVFQYREKAYFC within the central cavity of PEX9/blade IV is a binding site for α4β1 integrin. Treatment with synthetic peptide was found to prevent B-cell chronic lymphocytic leukemia transendothelial cell migration and survival.[21, 22] Mutation of either aspartic acid (Asp) residue (Asp-660 and Asp-663) in this peptide sequence abolished inhibition supporting the importance of Asp residues as key recognition sites for integrins.[23, 24] Furthermore, the LDT motif in this peptide sequence is a highly conserved motif found in a variety of well-known α4β1 integrin ligands.[23, 25, 26]

We previously utilized an *in silico* DOCKing approach for finding small molecules that bind to MMP-9 and identified a substituted pyrimidone, **1a,** which docked to the non-catalytic PEX domain of MMP-9.[27] Compound **1a** inhibited proMMP-9-mediated cancer cell migration and proliferation *in vitro*. Importantly, this compound did not inhibit MMP-9 enzymatic activity. Pyrimidone **1a** specifically binds to the hemopexin domain of MMP-9 and does not bind to closely related MMPs. In addition to inhibiting proMMP9-mediated cell migration, compound **1a** effectively prevented cancer metastasis in an *in vivo* mouse xenograft model.[27]

In this current study, we generated an *in silico* library of analogs of compound **1a** to find a more potent compound for potential clinical application. After screening for optimal DOCKing scores *in silico*, the top 14 compounds were synthesized and tested in a 2-D collagen dot migration assay. A high nanomolar inhibitor that maintained MMP specificity was identified (compound **3c**). Our data demonstrate that PEX-9 inhibitor **3c** selectively inhibits cell migration induced by proMMP-9 leading to reduced cell invasion predominately through disruption of

α4β1 integrin focal adhesion complexes. Thus PEX-9 inhibitors rectify the abnormal migratory phenotype associated with high MMP-9 expression.

RESULTS

Development of a second generation hit compound. We designed analogs of compound **1a** based on possible derivative syntheses that utilized an amide and a thioether coupling. Thus, three moieties were varied: the amine (R^1), the linker ($[CH_2]_n$), and the sulfhydrylpyrimidone (R^2) (Scheme). To rationally prioritize the synthesis of compound **1a** analogs, the University of California San Francisco (UCSF) DOCK (6.7) algorithm was used to rank various structures for predicted binding affinity. The proposed inhibitors were DOCKed to the PEX-9 domain pocket (PDB Code 1ITV) (**Fig. 1A and 1B**). This pocket is at the center of the four blades of the hemopexin domain.

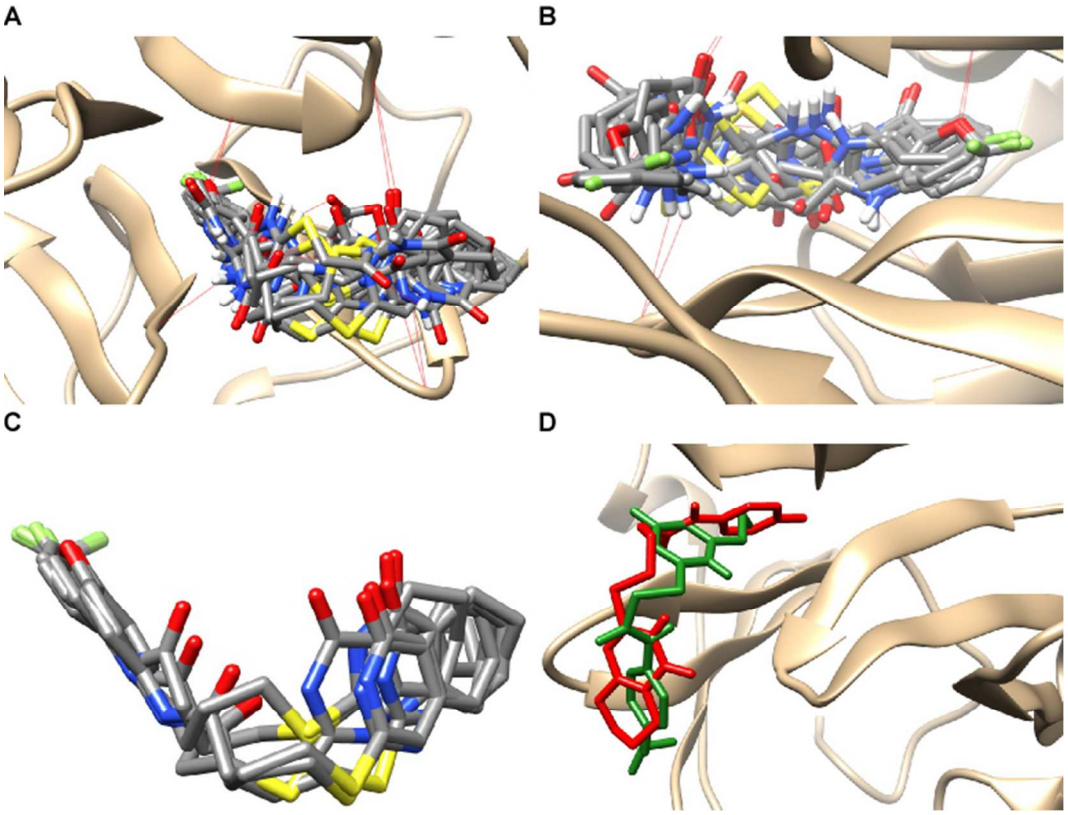

Fig. 1. PEX-9 inhibitor DOCKing to PEX-9 and binding site analysis. (A – B) PEX-9 inhibitor derivatives were DOCKed within the central cavity of the hemopexin domain of PEX-9 MMP-9 and hydrogen bonding was

visualized with dashed red lines. (C) A cluster of top hit compounds (**2c**, **3b**, **3c**, **3a**, **4a**, **4d**) were found to share a similar binding orientation. (D) The binding orientation of compound **1a** (green) relative to compound **3c** (red).

Amongst a library of 66 analogs, 14 (compounds **1a-d**, **2a, 2c**, **3a-d, 4a-e**) were chosen for synthesis based on superior DOCK algorithm scores (**Scheme**, **Table S1**). One motif that demonstrated consistent improvement in predicted binding affinity was modification of the 6-propylpyrimidone group to bicyclic pyrimidone systems.

*Chemical synthesis of PEX-9 parental compound **1a** and analogs.* First, the early lead compound **1a** was re-synthesized to confirm the chemical structure based on full characterization, using the synthetic route shown in the Scheme. The synthesis commenced with the reaction of aniline **5a** with bromoacetic acid in the presence of EDC·HCl to afford bromoacetanilide **6a** as white solid in 67% yield. Subsequently, **6a** was reacted with thiouracil **7** in aqueous NaOH and heated to 70 ^{o}C for 48 hours to give compound **1a** in 63% yield as a white solid after recrystallization. In addition, newly designed compounds **1b** and **1c** were synthesized using the same synthetic process (**Scheme**).

Closely related compound **1d** bearing a benzimidazole group was synthesized using a different route. In this synthesis, thiouracil **7** was converted to the corresponding thioacetic acid **8**, followed by the amide coupling with 2-aminobenzimidazole to give compound **1d** in modest yield. The attempted preparation of 2-bromoacetylaminobenzimidazole, following the synthetic route for compound **1a** did not yield pure compound. Thus, we judged that the synthetic strategy which coupled R^1 last would enable a better modular synthesis of analogs.

With this modular synthesis protocol in hand, we undertook synthesis of the analogs based on the original R^1 moiety and two bicyclic sulfhydrylpyrimidones, as well as the linkers with different lengths and a variety of aromatic R^2 substituents. Synthesis of compounds **2a** and **2c** followed the same strategy as that for compound **1d** by converting **7** to the corresponding thiobutanoic acid **9**, followed by amide formation by coupling with 4-substituted

Scheme. Synthesis of Inhibitors

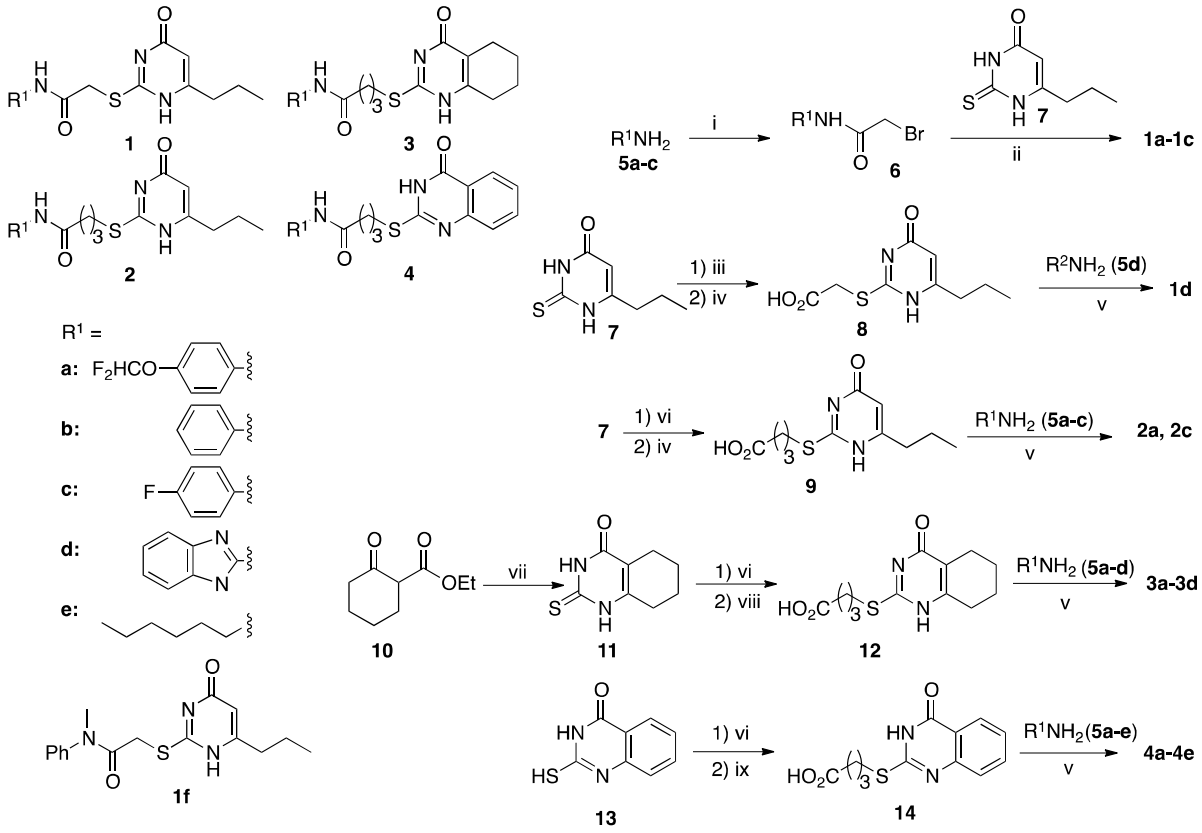

Reagents and conditions: (i) 2-bromoacetic acid, EDC·HCl, DCM, room temp. 24 h: 67% for **6a**, 47% for **6c**, 28% for **6b**; (ii) NaOH, H_2O, THF, 70 ^oC, 2 h: 63% for **1a**, 35% for **1b**, and 69% for **1c**. (iii) Ethyl 2-bromoacetate, K_2CO_3, MeOH, H_2O, rt, 15 min, 67%; (iv) LiOH, MeOH, H_2O, rt, 2 days, 28% for **8**, 66% for **9**; (v) (a) EDC·HCl, DMAP, room temp. 24 h: 40% for **1d**, 41% for **2a**, 39% for **2c**, 52% for **3a**, 46% for **3b**, 70% for **3c**, 22% for **3d**, 36% for **4b**, 46% for **4c**, 42% for **4a**, 26% for **4d**; (b) CDI, room temp., 24 h, 45% for **4e**. (vi) methyl 4-bromobutanoate, K_2CO_3, MeOH, H_2O, reflux: 47% for **9** (overnight), 73% for **12** (overnight), 81% for **14** (1 h); (vii) thiourea, MeONa, MeOH, reflux, overnight, 93%; (viii) NaOH, EtOH, RT, overnight, 99%; %; (ix) LiOH, DMSO, H_2O, room temp., 2h, 86%.

anilines **5a** and **5c** to give **2a** and **2c** in modest yields.

In a similar manner, compounds **3a-d** were synthesized in moderate yields through the coupling of anilines and 2-aminobenzimidazole with thiobutanoic acid **12**, prepared from 2-sulfhydryl-5,6,7,8-tetrahydroquinazolin-4(3H)-one (**11**) as shown. Compound **11** was readily prepared by reacting keto ester **10** with thiourea and a base. Compounds **4a-e** were synthesized in moderate yields using the same strategy except for starting from 2-sulfhydryltetrahydroquinazolinone (**13**) and employed anilines and 2-aminoimidazole for the amide formation.

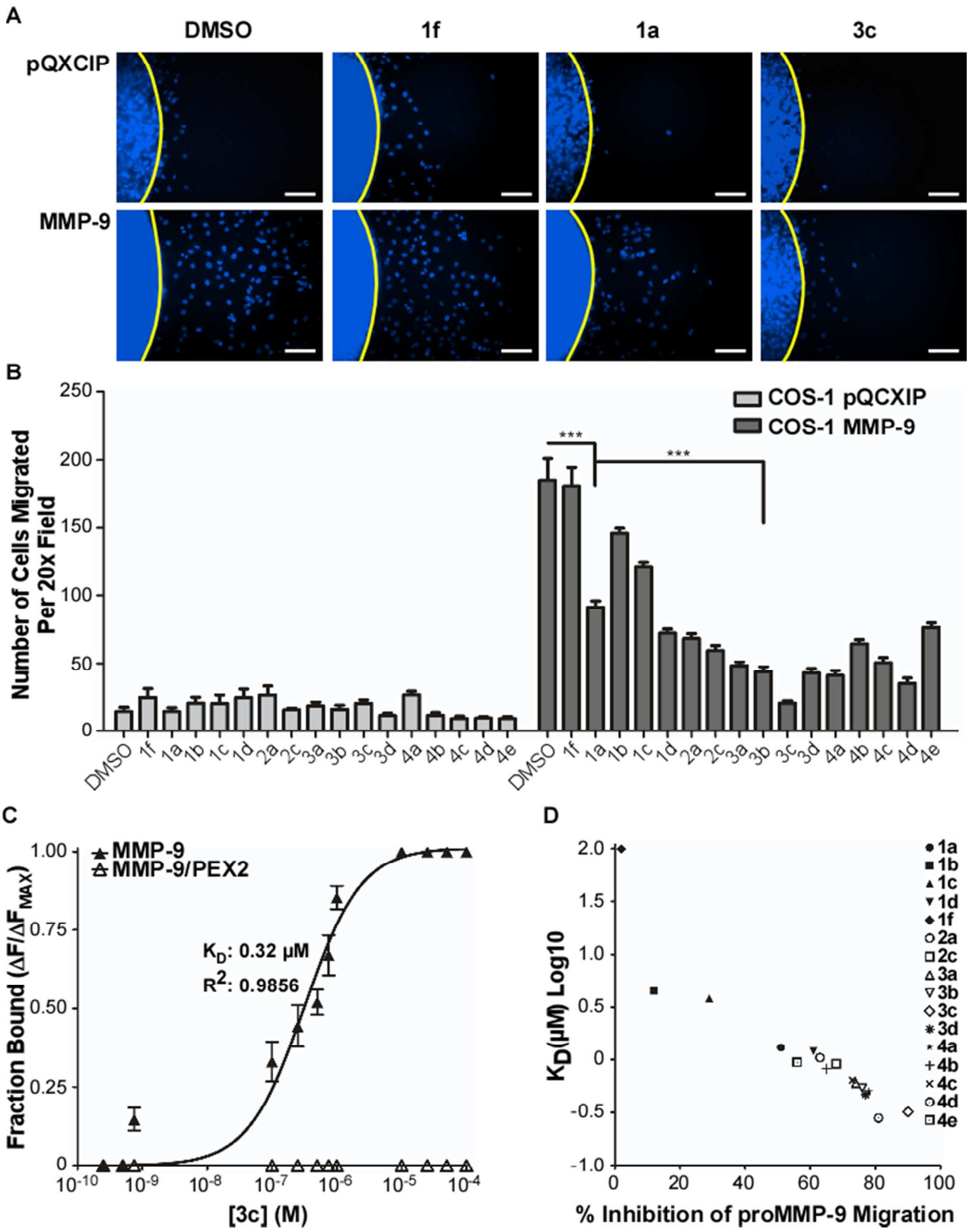

Fig. 2. Structure activity relationship analysis of all synthesized PEX-9 inhibitor derivatives. (A) Representative 20x magnification DAPI images of COS-1 cells engineered to stably express either vector control or proMMP-9 cDNA vectors in a two-dimensional migration assay after treatment with 50 μM of **1f, 1a,** or **3c**. Scale bar = 250 *μ*m. (B) Quantitative analysis of migrated COS-1 vector control and proMMP-9 expressing cells after treatment with 50 μM of inhibitors. (C) Tryptophan fluorescence emission of proMMP-9 or proMMP-9/PEX2

(ex 280 nm, em 330 nm) was monitored and inhibitor **3c** titrated into the protein solution. A maximal λ_{Max} shift of 9 nm was observed after treatment with 25 μM inhibitor. Solid line is a curve fit for Kd for compound **3c** was determined. (D) Kd for each inhibitor was plotted against percent inhibition of proMMP9-mediated cell migration for each inhibitor.

Structure activity relationship analysis of PEX-9 derivative compounds. COS-1 cells were chosen for this set of experiments due to their low migratory capacity and complete lack of MMP-9 expression thereby minimizing potential artifacts when interpreting the data. Overexpression of proMMP-9 results in enhanced cell migration in a two-dimensional dot migration assay.[27] This assay was initially used to test the efficacy of analogs at a single concentration, 50 μM. This concentration was used as a maximal cutoff because concentrations above 50 μM compound **1a** did not increase inhibitor effectiveness in COS-1 cells.

Cells were mixed with type I collagen solution with or without compound, dotted onto a 96-well plate, and allowed to migrate for 18 hours. They were then fixed, stained and scored for extent of migration (**Fig. 2A and 2B**). 2-(4-Oxo-6-propyl-1,4-dihydropyrimidin-2-ylthio)-*N*(methyl)-phenylacetamide (**1f**) was used as a negative control.[27] Compound **3c** was the most effective and was selected for further study. The migration assay was repeated in HT1080 fibrosarcoma cells, which endogenously express MMP-9, and the same inhibition potency was observed for both compound **1a** and **3c** relative to control groups (**Supplemental Fig. 1A and 1B**).

Compound affinity for PEX-9 binding. A blue shift in proMMP-9 tryptophan fluorescence was monitored to determine the binding affinity of all derivative compounds as previously described.[27] The Kd for compound **3c** binding to proMMP-9 is 0.32 μM (**Fig. 2C**), four times tighter than parent compound **1a**. Moreover, a clear correlation between binding affinity and inhibition potency in the migration assay was observed (**Fig 2D**). Thus, the biophysical SAR is maintained in the cellular assay and increased inhibition of cell migration is MMP9-dependent and due to optimization of chemical structure for binding the PEX-9 domain.

PEX-9 binding specificity. A chimera of proMMP-9 and MMP-2 in which the MMP-9 PEX domain was replaced by that of MMP-2, (proMMP-9/MMP-2PEX)[11] was tested for analog binding. The tryptophans in MMP-9 PEX domain are conserved in the MMP-2 PEX domain. Upon titration of compound **3c** with the chimera, no shift in fluorescence was observed suggesting that **3c** does not bind to MMP2-PEX (**Fig. 2C**).

As an additional test of binding selectivity, saturated transfer difference (STD) NMR was performed with purified recombinant proMMP-2 and proMMP-9 protein. ProMMP-2 and proMMP-9 are highly similar in structure and function, belonging to the same subfamily of MMPs known as the type IV collagenases and/or gelatinases. Thus proMMP-2 constitutes the best control for testing the selectivity of the PEX-9 inhibitor.[28] Selective saturation of the 1.12 ppm resonance (proMMP-2 and proMMP-9) was used for STD NMR spectra. STD peaks were observed in the presence of proMMP-9, but not in the presence of proMMP-2, indicating that derivative compound **3c** is specific for the PEX-9 target (**Supplemental Fig. 2A - 2F**). Thus, binding specificity is maintained upon increasing binding affinity.

PEX-9 inhibitor target specificity. To test whether compound **3c** is specific for inhibiting only proMMP9-mediated migration, a two-dimensional dot migration assay was performed using COS-1 cells engineered to stably express vector control pQCXIP, proMMP-2, proMMP-9, or proMMP-14 cDNA vectors (**Fig. 3A**). An immunoblot was performed to confirm protein expression and proper localization of each MMP (MMP-2/-9 are secreted while MMP-14 is membrane bound) (**Fig. 3B**). As expected, expression of these three MMPs resulted in enhanced cellular migration in COS-1 cells.[11] Treatment with either compound **1a** or **3c** only inhibited proMMP9-mediated migration: compound **3c** was significantly more effective at inhibiting migration (**Fig. 3C**).

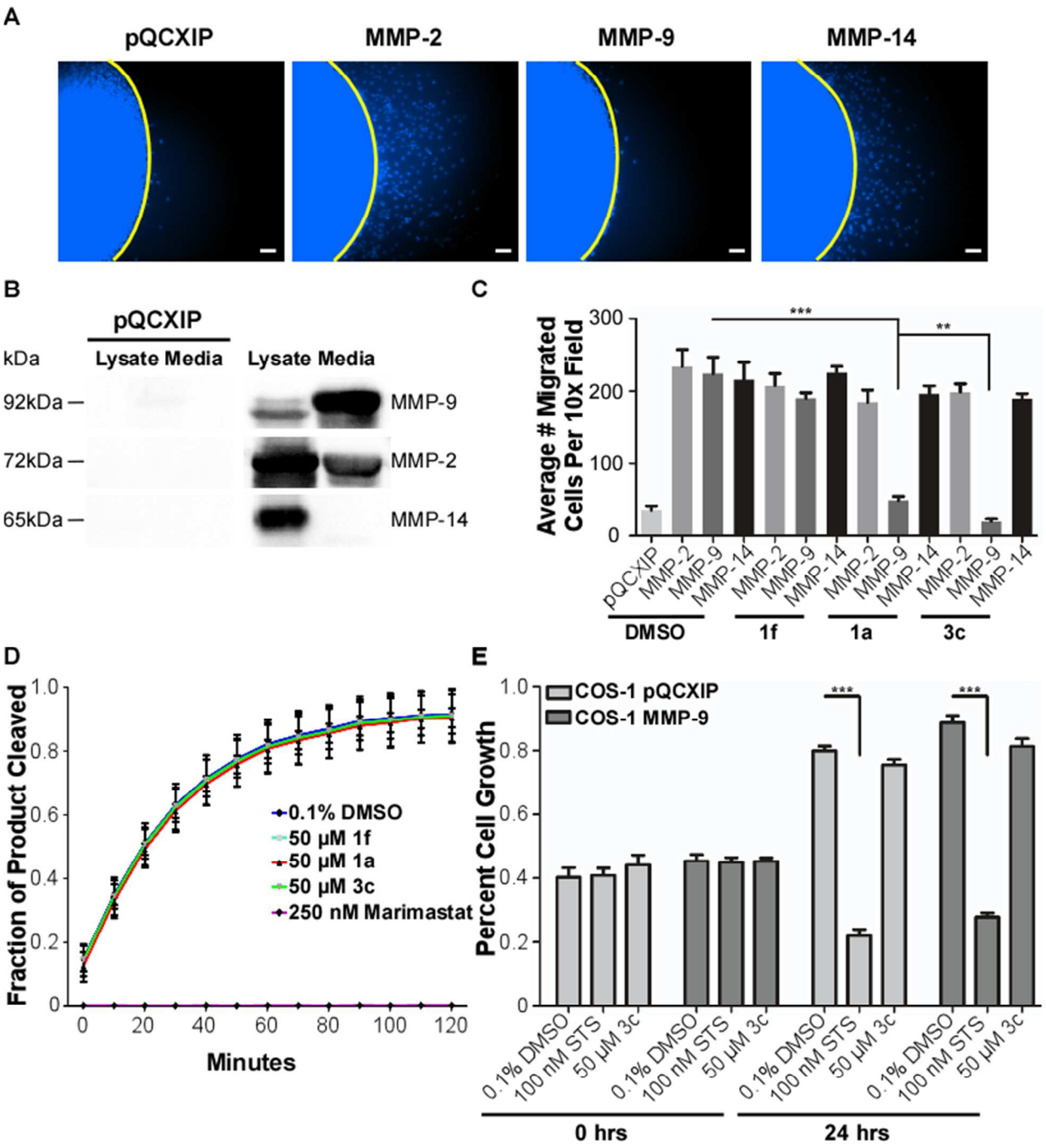

Fig. 3. Determination of PEX-9 inhibitor specificity in the presence of homologous and non-homologous MMPs. (A) COS-1 cells transiently transfected with either vector control, proMMP-2, proMMP-9, or MMP-14 cDNAs were treated with 50 μM compound **3c** and then used in a two-dimensional dot migration assay. Representative 10x DAPI magnification images were taken and are shown. Scale bar = 250 μm. (B) MMP expression and proper localization was confirmed by immunoblot analysis of cell lysates and protein precipitated serum-free medium. pQCXIP is the vector only control. (C) Quantification of inhibition proMMP-9 mediated cell migration by compounds **1a** and **3c.** Compound **1f** was used as a negative control. (D) Assay of MMP-9 catalytic activity using a fluorogenic peptide degradation assay and activated MMP-9. proMMP-9 protein was activated with 1 mM APMA overnight. 100 ng of activated MMP-9 was incubated with 10 μM fluorogenic peptide (excitation- 320 nm; emission- 405 nm) in the presence of buffer, 50 μM compound **1a**, **3c, 1f, or** 250 nM broad-spectrum catalytic inhibitor Marimastat. Readings were performed every 10 minutes over the course of 2 hours. (E) Cell viability was assayed with MTT. COS-1 cells engineered to stably express either vector control or proMMP-9 cDNA were treated for 24 hours with DMSO control, 50 μM compound **3c** or 100 nM staurosporine (STS) as a positive control for acute cell toxicity.

Effect of PEX-9 inhibitor on MMP-9 catalytic activity. Recombinant proMMP-9 protein was purified and incubated overnight in a 37 ^{o}C water bath in TNC buffer + 1 mM APMA to artificially activate the protein.[29, 30] The next day, the purified protein was incubated with 10 μM fluorogenic peptide (Mca-Pro-Leu-Gly-Leu-Dpa-Ala-Arg-NH2), and catalytic activity was monitored over 2 hours in the presence of compounds **1a**, **3c**, **1f**, and marimastat, a broad-spectrum MMP catalytic inhibitor. No inhibition of the catalytic activity was observed with **1a** or **3c**, corroborating that PEX-9 inhibitors do not modulate the catalytic activity of the protease. In the presence of marimastat (K_d = 80 nM) no substrate cleavage was observed (**Fig. 3D**). Therefore, inhibition of proMMP9-mediated cell migration by compound **1a** or **3c** is not due to loss of proteolytic activity.

Cell viability analysis. Compound **3c** was evaluated for acute cytotoxicity. COS-1 cells stably expressing either vector control or proMMP-9 cDNA were treated with 50 μM **3c** for 24 hours. As negative and positive controls, cells were treated with DMSO alone or 100 nM staurosporine (STS), an apoptosis inducer, respectively.[31] Significant cell death was only observed after treatment with STS. A non-statistically significant 8% decrease in cell growth occurred after treatment with 50 μM of compound **3c** (**Fig. 3E**). These experiments were repeated in endogenous MMP-9 expressing HT1080 fibrosarcoma cells, which were analyzed for chronic toxicity (cells were re-treated every three days for a total of nine days). No cell death was observed at 100 μM **3c** (*data not shown*).

PEX-9 inhibitors decrease MMP-9 dimer formation and association with EGFR. Human fibroscarcoma HT1080 cells were co-transfected with MMP-9 cDNAs tagged with either a Myc or HA tag as previously reported.[12] The next day, cells were switched to serum free media and treated with 50 μM of either compound **1a** or **3c** overnight. Using Myc antibody for immunoprecipitation and HA antibody for immunoblotting, the formation of dimeric MMP-9 was monitored. Compound **3c** significantly blocked MMP-9 dimer formation as compared to control

compound **1f.** In addition, inhibition of PEX-9 with **1a** or **3c** reduced endogenous CD44 and EGFR co-immunoprecipitation (**Supplemental Fig. 3A**). Moreover, these PEX-9 inhibitors reduced phosphorylation of $EGFR^{Tyr1068}$ and its downstream targets AKT^{Ser473} and $Erk1/2^{Thr202/Tyr204}$ (**Supplemental Fig. 3B**).

PEX-9 inhibitors disrupt MMP-9 interaction with α4β1 integrin. HT1080 cells transiently co-transfected with tagged MMP-9 cDNAs were prepared as described above.[12] Inhibition of PEX-9 with 50 μM of either compound **1a** or **3c** reduced endogenous $\alpha4\beta1$ integrin co-immunoprecipitation (**Fig. 4A**). Inhibition of PEX-9 with 50 μM of either compound **1a** or **3c** reduced Src^{Tyr418} phosphorylation in addition to phosphorylation of Src downstream targets $FAK^{Tyr\ 576/577}$ and PAX^{Tyr118} (**Fig. 4B**.)

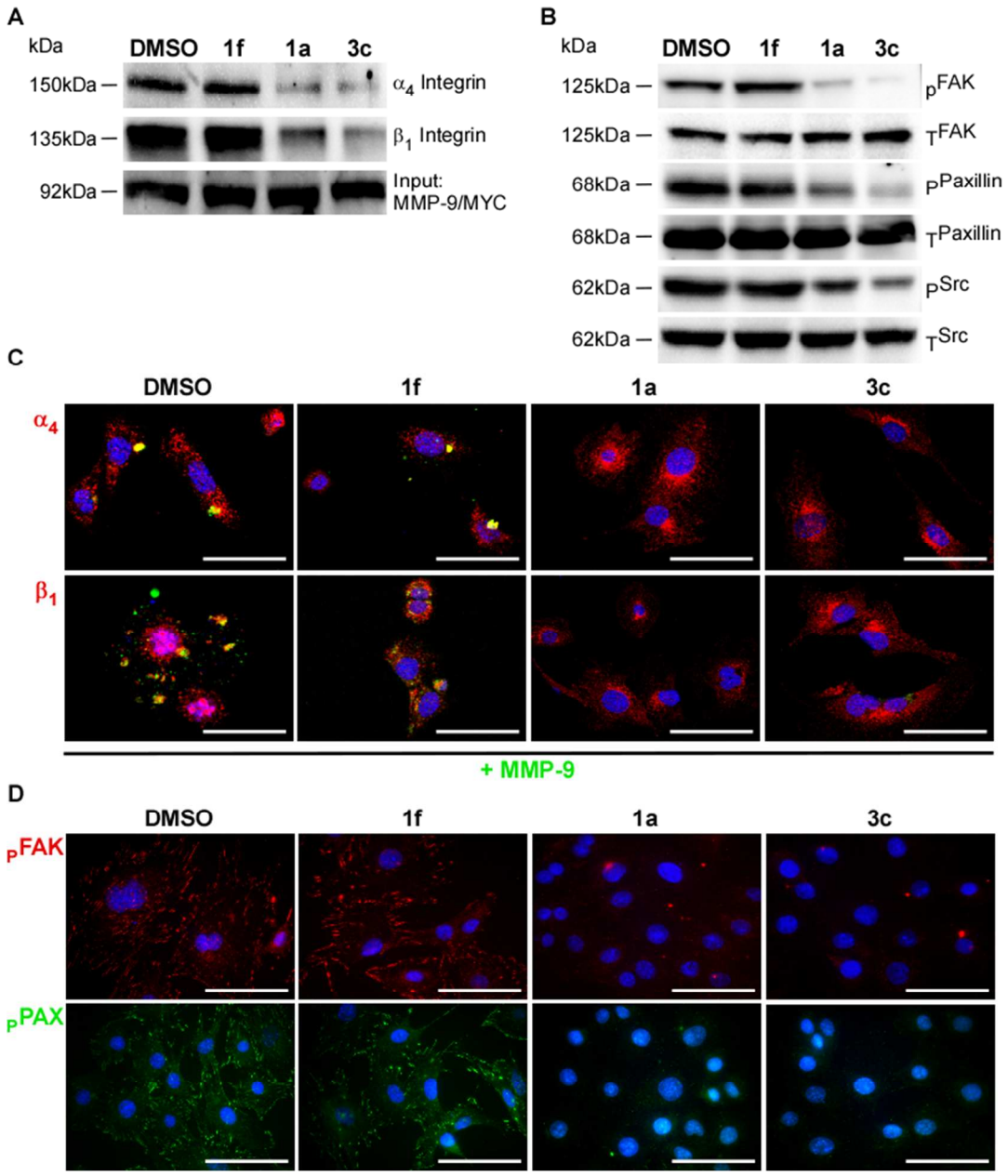

Fig. 4. Treatment with PEX-9 inhibitor results in decreased interaction between MMP-9 and α4β1 integrin and attenuated downstream signaling. (A) Co-IP with HT1080 cells transiently overexpressing MMP-9/MYC cDNA was performed in the presence of 50 μM compound **3c**. MMP-9/MYC was immunoprecipitated using an anti-Myc antibody and served as an input control while α4 and β1 integrin interactions were probed via immunoblot. A decrease in MMP-9 interacting with both integrin subunits was observed as well as a (B) decrease in Src^{Tyr418} and downstream target proteins $FAK^{Tyr\ 576/577}$/PAX^{Tyr118} phosphorylation. (C) 60x confocal images were captured and representative images of MMP-9 (green) and each integrin subunit (red) were taken after treatment of HT1080 cells with 50 μM of either compound **1a** or **3c** compound **1f**. Scale bar = 100 *μ*m. (D) 60x confocal images were captured and representative images of p-$FAK^{Tyr\ 576/577}$ (red) and p-PAX^{Tyr118} (green) were taken after treatment of HT1080 cells with 50 μM of either compound **1a** or **3c** compound **1f**. Scale bar = 100 *μ*m.

Evaluation of MMP-9 cell surface localization upon treatment with PEX-9 inhibitors. HT1080 cells were fixed in 4% paraformaldehyde then subsequently incubated with anti-MMP-9 in addition to anti-α4 and/or β1 integrin antibodies to monitor relative levels of localization of

these proteins at the cell surface. The cells were counterstained with DAPI nuclear dye. Treatment with either compound **1a** or **3c** resulted in loss of MMP-9 from the cell surface (**Fig. 4C**). However, treatment with either solvent control DMSO or negative control compound **1f** did not disrupt the localization of MMP-9 on the cell surface.

Evaluation of focal adhesion complexes in the presence of PEX-9 inhibitors. HT1080 cells were fixed after overnight treatment with 50 μM PEX-9 inhibitors, probed for either $FAK^{Tyr\ 576/577}$ or PAX^{Tyr118} and counterstained with DAPI. A decrease in the formation of FAK and PAX adhesion junctions, normally depicted as "large punctae", was observed in cells after treatment with PEX-9 inhibitor compound **1a** or **3c** (**Fig. 4D**).

Validation of MMP-9's role in signaling. MMP-9 expression was silenced using an shRNA approach as previously described.[12] HT1080 cell lysates were collected and analyzed by immunoblot. Attenuation of MMP-9 expression resulted in a decrease in the phosphorylation of $EGFR^{Tyr1068}$, $FAK^{Tyr\ 576/577}$, PAX^{Tyr118}, Src^{Tyr418}, AKT^{Ser473}, and $Erk1/2^{Thr202/Tyr204}$ (**Supplemental Fig. 4A**). These findings are corroborated by Kinexus antibody microarray screening of phosphorylation-dependent signaling pathways in MMP-9-transfected COS-1 cells[12] in which Src, FAK, and PAX phosphorylation increase in proMMP-9 overexpressing cells (**Supplemental Figure 4B)**.

Treatment with PEX-9 inhibitor prevents association of EGFR with CD44 and β1 integrin. HT1080 cells were treated with 50 μM **3c**, **1a**, **1f** or DMSO alone. Cell lysates were collected and analyzed by a co-IP assay in which endogenous EGFR was captured with an anti-EGFR antibody and served as an input control. CD44 and β1 integrin were individually probed on the immunoblot. Decreased interaction between EGFR-CD44 and EGFR-β1 integrin was observed after treatment with **3c** (**Supplemental Fig. 5A**).

Src activation is a PEX-9 dependent process. Non-MMP-9 expressing MCF-7 breast cancer cells were transiently transfected with either vector control pcDNA3.1, proMMP-9, or

chimeric proMMP-9/MMP-2PEX cDNA constructs. Phosphorylation of Src^{Tyr418} was detected using an immunoblotting assay. Increased Src^{Tyr418} phosphorylation was observed in proMMP-9 overexpressing cells. PEX domain swapping with MMP-2 has no effect on Src^{Tyr418} phosphorylation similar to vector control pcDNA3.1 expressing cells (**Supplemental Fig. 5B**).

Effect of PEX-9 inhibitors on cell adhesion. A 96-well plate was coated with a thin layer of either collagen or fibronectin (5 µg/ml in PBS) substrate before use. HT1080 cells were then seeded onto wells and incubated at 37 ^{o}C for 30 min in the presence of various inhibitors. Wells were washed and cells were fixed in 4% paraformaldehyde and stained with DAPI. Images of each 96-well were microscopically captured and counted for the number of cells still adherent to the coated surface using automated computer software. Compound **1a** or **3c** inhibited cellular adhesion whereas treatment with Marimastat, a broad-spectrum MMP catalytic inhibitor, had no observable effect on cell attachment. Solvent DMSO and compound **1f** also had no affect on cell adhesion (**Supplemental Fig. 6A**).

Effect of broad-spectrum MMP catalytic inhibitor marimastat on focal adhesion complexes. HT1080 cells treated with 80 nM of broad-spectrum MMP inhibitor marimastat were analyzed by immunofluorescence microscopy for both p-$FAK^{Tyr\ 576/577}$ and p-PAX^{Tyr118}. Treatment with marimastat did not prevent the formation of focal adhesion contact sites in HT1080 cells (**Supplemental Fig. 6B**).

Treatment with PEX-9 inhibitor prevents both angiogenesis and invasion in a chorioallantoic membrane (CAM) assay. A CAM assay was carried out to evaluate angiogenic and invasive potential of HT1080 cells after treatment with **3c**. HT1080 cells were adsorbed onto a gelatin sponge and implanted onto the surface of the chicken embryo CAM followed by treatment with 100 µM stock solution compound **1f**, compound **1a** or **3c** (final drug concentration is estimated to be 0.5 µM). After a 4-day incubation, neovascularization was imaged and quantified. Treatment with either compound **1a** or **3c** significantly reduced the

angiogenic potential of HT1080 cells as compared to solvent DMSO and negative compound **1f** control treated cells (**Fig. 5A - 5B**).

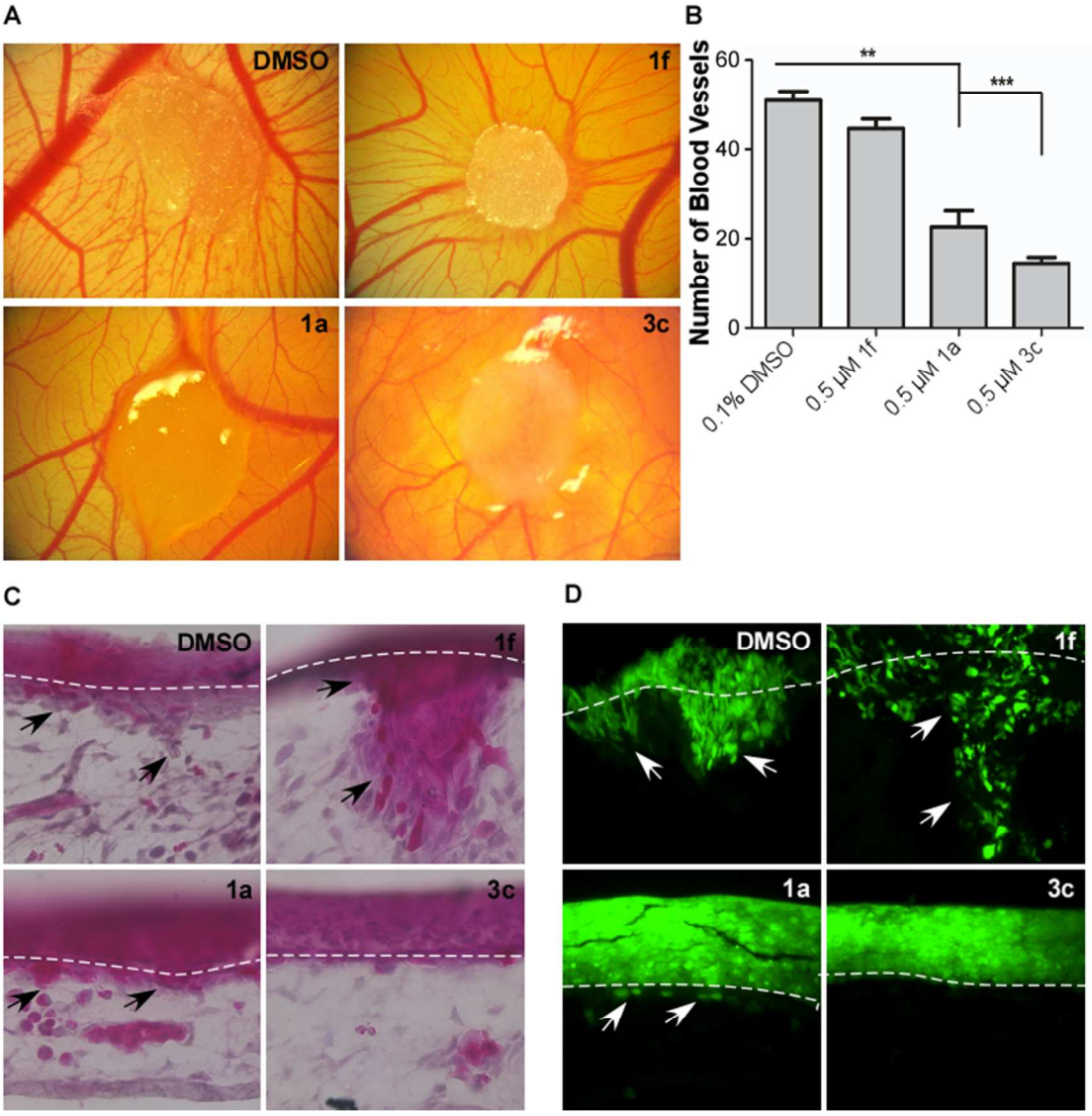

Fig. 5. Compound 3c prevents angiogenesis and invasion through the basement membrane in a CAM assay. (A) HT1080 cells were adsorbed onto a gelatin sponge, implanted atop the CAM, and were then subsequently treated with DMSO control, 0.5 μM compound **1f**, **1a**, or **3c**. After 4 days of incubation at 37 ^{o}C, representative images of the angiogenic bed surrounding the gelatin sponge were taken. (B) Analysis and quantification of the number of blood vessels in the area surrounding the implanted sponge. (C - D) The CAM was inoculated with HT1080 GFP^{+} cells mixed with a type I collagen solution and treated with DMSO control, 0.5 μM compound **1f**, **1a**, or **3c.** After 7 days of incubation at 37 ^{o}C, CAM membranes were isolated, sectioned, H&E stained, and imaged under 20x magnification.

HT1080 cells stably expressing GFP were mixed with a type I collagen solution (3 mg/mL) and seeded atop the CAM to ensure the cells localized to a specific area. Then they were treated with a 100 μM stock solution of compound **1f**, compound **1a** or **3c** (final drug

concentration is estimated to be 0.5 μM). The invasion of cancer cells through the epithelium and basement membrane of the upper CAM into connecting tissue was examined by hematoxylin and eosin staining (**Fig. 5C**) in addition to fluorescence microscopy for GFP^+ cells (**Fig. 5D**). Treatment of HT1080 cells with either compound **1a** or **3c** reduced invasion of CAM tissue compared to treatment with either DMSO or compound **1f** control.

DISCUSSION

MMPs are crucial for the degradation of ECM and blood vessel linings. Degradation allows tumor cells to escape their primary location and enter the circulatory system where they can travel to seed secondary tumors elsewhere in the body.[32, 33] Therefore, targeting MMPs with inhibitors is of interest for cancer drug development.[34] Original inhibition attempts focused on synthetic collagen-mimicking hydroxamate inhibitors that chelate the zinc ion in the active site upon binding.[35] These drugs largely failed in clinical trials due to lack of selectivity for individual MMPs. Due to the specificity issues inherent in generating inhibitors of MMP proteolytic activity, we developed inhibitors which target MMP-9's hemopexin domain. MMP hemopexin domains share a common tertiary structure, yet the surface residues of MMP hemopexin domains are distinct and one hemopexin domain cannot functionally substitute for another.

Identification of a more potent PEX-9 inhibitor. To identify compounds that bind more tightly to the hemopexin domain of MMP-9 than our original hit,[27] structural diversity was introduced at three positions and computational DOCKing utilized to prioritize synthesis and testing of a small subset. The similarities between their predicted and measured binding affinities indicate that the DOCKed structures may be used to infer important binding modalities. Compounds that displayed the greatest inhibition of proMMP-9 mediated migration had longer linkers with three methylenes between the amide and the sulfide moieties and at

least 1 fluorine in the R^1 group. A cluster of derivative compounds (**2c, 3a-c, 4a, 4d**), shared a similar binding geometry within the hemopexin domain of MMP-9 (**Fig. 1C**). In all the tightest binding PEX-9 inhibitor derivatives, the aryl fluorine atoms were found deep within the binding pocket in contrast to the original hit **1a**, in which the difluoromethoxyphenol moiety remained solvent exposed. The STD-NMR data support the binding pose in which the aniline is deeply buried in the pocket (**Supplemental Fig 2A-F**). In addition, fusion of a second ring to the pyrimidone moiety to form a quinazolinone significantly improved inhibitor efficiency and affinity. The length of the aliphatic chain between the two ring moieties is key for optimizing binding interactions. Comparison of DOCKed compounds **1a** and **3c** highlights differences in binding orientation that may contribute to the higher affinity of **3c** (**Fig. 1D**).

Binding affinity for PEX-9 correlates with inhibition of proMMP9-mediated migration (**Fig. 2D**) across our 16-compound series that spans 1.5 logs of binding affinity. These structure-activity results support that the mechanism of inhibition of proMMP9-dependent cell migration is through targeting PEX-9 on the cell surface.

proMMP-9 homodimerization is a critical step for interaction with CD44 at the cell surface which results in decreased phosphorylation of $EGFR^{Tyr1068}$ and its downstream targets AKT^{Ser473} and Erk $1/2^{Thr202/Tyr204}$ phosphorylation.[12] Compound **3c** demonstrated enhanced efficacy of blocking proMMP-9 homodimerization and activation of downstream protein targets (**Fig 4, Supplemental Fig. 3)**. Moreover, our most potent compound, **3c,** retained specificity for a single MMP as demonstrated by the lack of inhibition in proMMP-2 or proMMP-14 mediated cell migration (**Fig. 3C**). Our structure activity correlation (Fig. **2D)** and the specificity of inhibition for proMMP-9 mediated cell migration corroborate that compound **3c** targets PEX-9 *in vitro* and *in vivo* and not a downstream signaling target common to other mediators of cell migration.

Recently Garcia-Pardo and coworkers reported that the central cavity of PEX-9 interacts with α4β1 integrin as a mechanism for cross-talk between MMPs and integrin focal adhesion formation.[17, 18, 21] In turn, Src kinase interacts with the cytoplasmic tail of α4β1 integrin subunits, which is critical for integrin function to promote and regulate focal adhesion turnover.[36-42] Interestingly, PEX9-α4β1 integrin downstream signaling increases activation of Fyn, a Src family kinase, and drives chronic lymphocytic leukemia B cell survival.[17] Therefore, we examined the consequences of binding **3c** to PEX-9 on α4β1 integrin-mediated Src signaling.

Using a co-immunoprecipitation approach, we found that PEX-9 inhibitors interfere with binding between proMMP-9 and α4β1 integrin and can block cross-talk signaling. This disruption is accompanied by decreases in phosphorylation levels of Src^{Tyr418} and its downstream substrates $FAK^{Tyr\ 576/577}$ and PAX^{Tyr118} (**Fig. 4B)**. Immunofluorescence imaging in HT1080 cells further supported the idea that focal adhesion junctions ("large punctae") were lost upon treatment with PEX-9 inhibitor (**Fig. 4C-D**). We also demonstrated that overexpression of proMMP-9 in MCF-7 breast cancer cells enhanced Src activation. Overexpression of proMMP-9/MMP2-PEX in MCF-7 breast cancer cells or silencing of endogenous MMP-9 expression in HT1080 attenuated Src activation. Taken together, the data suggest that the proMMP-9 hemopexin domain is required for enhanced cellular adhesion and migration.

Potential mechanism by which Src is activated. Our data are in agreement with the literature showing that α4β1 integrin clustering is sufficient for activation of Src kinase.[37, 43] However, in addition to integrin clustering, EGFR can directly activate Src kinase and EGFR interacts with β1 integrin.[44-46]

It is proposed that proMMP-9 forms a large charged surface for complex interactions with multiple surface proteins involved in outside-in signaling.[47] The hemopexin domain of

proMMP-9 may act as a scaffold to enhance clustering of α4β1 integrin-EGFR-CD44 at the cell surface and result in aberrant Src activation.[48] Garcia-Pardo and coworkers demonstrated that a peptide mimicking blade 1 of PEX-9 inhibits interaction with integrin, and that a second peptide mimicking blade 4 of PEX-9 inhibits interaction with CD44.[21, 22] We reasoned that our inhibitor which binds directly to PEX-9 could simultaneously disrupt both interactions. Indeed, our co-immunoprecipitation experiments demonstrate that addition of **3c** selectively disrupts proMMP-9 interaction with both α4β1 integrin (**Fig. 4)** and CD44 (**Supplemental Fig. S3).**

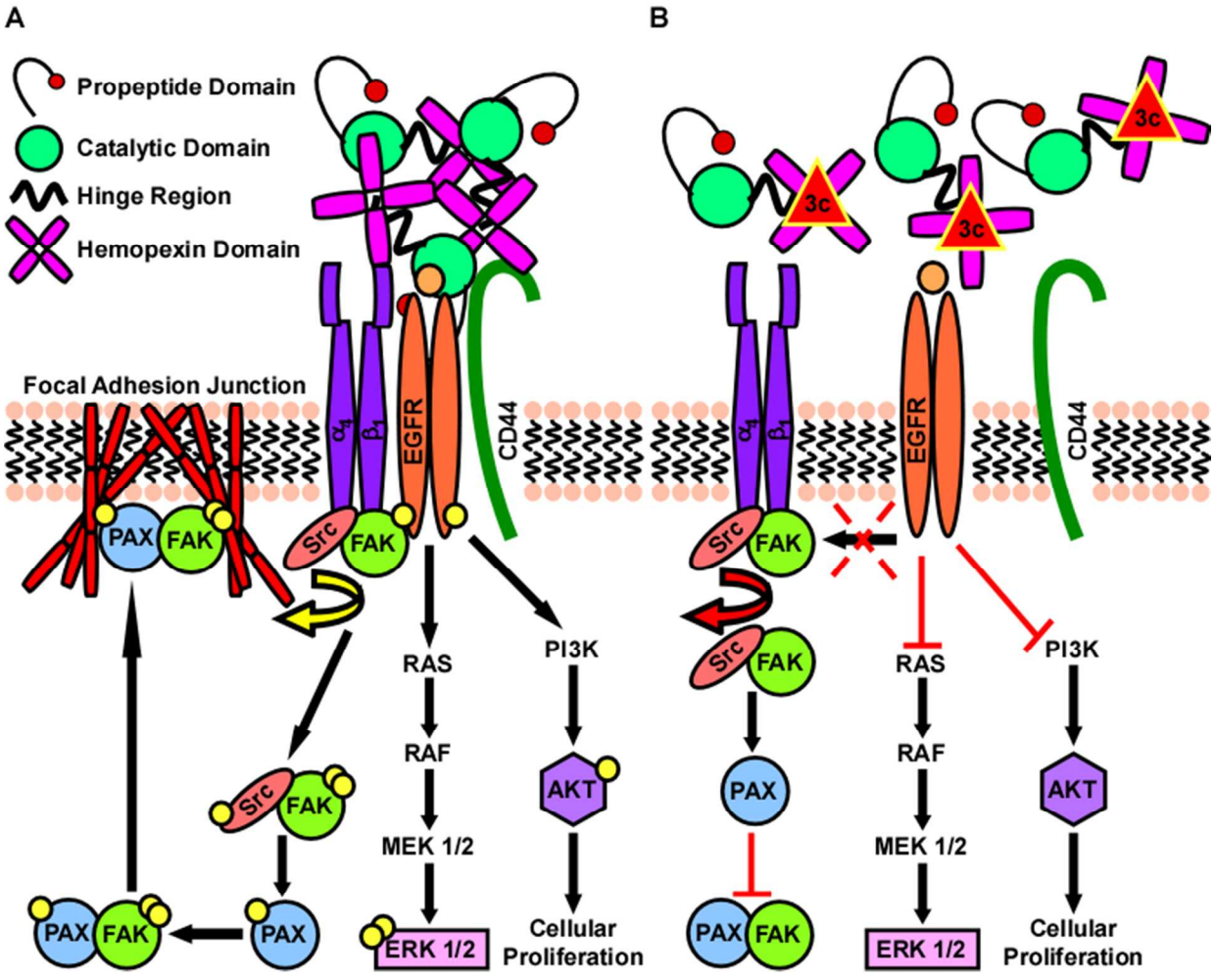

Fig. 6. Overview of the mechanism by which MMP-9 regulates formation of focal adhesion junctions. (A) During exocytosis and upon being secreted into the extracellular space, proMMP-9 forms a large complex with itself that can then act as a scaffold for promoting outside-in signaling. In our model, PEX-9 scaffolding promotes the association of β1 integrin-EGFR-CD44. Interaction with CD44 results in enhanced EGFR activation in addition to increased phosphorylation of its downstream targets AKT and Erk 1 + 2 (through the MAPK/Erk pathway).

While complexed to β1 integrin, EGFR then goes on to transactivate Src kinase after it is recruited to the α4 integrin subunit during the generation of a new focal adhesion contact site. After activation, Src can then directly phosphorylate FAK currently associated to the β1 integrin subunit resulting in its maximal catalytic activity. This active Src-FAK complex can then bind and activate PAX resulting in a mature FAK-PAX complex necessary for the formation of focal adhesion junctions. Formation of a complex between FAK and PAX results in final translocation to ECM-integrin junctions at the cell surface where they regulate cytoskeletal interactions resulting in enhanced cellular adhesion, migration, and invasion of cancer cells. (B) Treatment with PEX-9 inhibitor (depicted as red triangle) prevents MMP-9 scaffolding thereby preventing downstream signaling driven by EGFR activation.

Importantly, our inhibitor is specific for MMP-9. Targeting the hemopexin domain to investigate the role of MMP-9 in promoting cellular adhesion has identified a connection to integrin and Src in a complex adhesion network as depicted in **Figure 6**. There are currently no effective cancer therapeutics designed to target adhesion receptors because cancer cells can change the mechanism by which they migrate depending upon their environmental constraints.[49] Our *in vivo* CAM experiments demonstrate that we can inhibit two key determinants of tumor cell metastatic potential, angiogenesis and invasion (**Fig. 5**), through PEX domain targeting. Our small molecule inhibitor paves the way for designing new therapeutic strategies for the treatment of metastatic disease and opens the door for the future development of new technologies and tools for understanding the role of individual MMPs in cancer progression. Development of PEX inhibitors for other MMPs will provide understanding of their non-catalytic functions and a strategy for reducing undesirable off-target effects previously observed in broad-spectrum MMP catalytic inhibitor clinical trials.

EXPERIMENTAL METHODS

Materials. Collagen type I (acetic acid-extracted native type I collagen from rat tail tendon) was obtained from BD Bioscience Discovery Labware (Franklin Lakes, NJ). Fibronectin solution was purchased from Sigma-Aldrich (St. Louis, MO). Hoechst nuclear stain was obtained from Invitrogen (Grand Island, NY). Rabbit anti–p-AKT^{Ser473}, anti-AKT (total), anti-β1 integrin, anti-p-Erk1/2$^{Thr202/Tyr204}$, anti-p-FAK$^{Tyr\ 576/577}$, anti-FAK (total), anti-p-PAX^{Tyr118}, anti-PAX (total) and anti-EGFR (total) antibodies were all purchased from Cell Signaling

Technology (Danvers, MA). Mouse anti-Erk1/2 (total), anti-β-actin and anti–α/β-tubulin antibodies were also purchased from Cell Signaling Technology (Danvers, MA). Rabbit anti-p-Src^{Tyr418} and anti-Src (total) in addition to mouse anti-β1 integrin were obtained from Abcam (Cambridge, MA). Mouse anti-α4 integrin and anti-CD44 in addition to rabbit anti-α4 integrin were purchased from Santa Cruz Biotechnology (Santa Cruz, CA). Rabbit anti-MMP-9 was purchased from Millipore (Darmstadt, Germany). Rabbit p-EGFR^{Tyr1068} was obtained from Enzo Life Sciences (Ann Arbor, MI). Rat anti-CD44 was obtained through BD Pharmingen (San Diego, CA). Mouse anti-HA was purchased from Invitrogen-ThermoFisher Scientific (Waltham, MA). Rabbit anti-MYC and anti-HA in addition to horseradish peroxidase conjugated anti-rabbit, anti-mouse, and anti-rat antibodies were obtained from Rockland Immunochemicals (Gilbertsville, PA). Mouse anti-MYC was purchased from Roche Life Sciences (Branford, CT). Alexa Fluor 488 and 568 anti-rabbit/-mouse antibodies were purchased from Molecular Probes, Life Technologies (Grand Island, NY). proMMP-9 used in kinetic experiments was purchased from Biolegends (San Diego, CA). Mca-PLGL-Dpa-AR-NH_2 Fluorogenic MMP Peptide Substrate was purchased from R&D Systems (Minneapolis, MN). Chemicals were purchased from Sigma-Aldrich, Fisher Scientific, and VWR International and used as received or purified before use by standard methods. Tetrahydrofuran was freshly distilled from sodium and benzophenone. Dichloromethane was also distilled immediately prior to use under nitrogen from calcium hydride. 2-(4-Oxo-6-propyl-1,4-dihydropyrimidin-2-ylthio)-*N*(methyl)-phenylacetamide (**1f**) was purchased from ChemBridge Corp. (San Diego, CA).

General Methods. ^{1}H and ^{13}C NMR spectra were measured on a Bruker 300, 400, 500, or 700 MHz spectrometer. Melting points were measured on a Thomas-Hoover capillary melting point apparatus and are uncorrected. TLC was performed on Sorbent Technologies aluminum-backed Silica G TLC plates (Sorbent Technologies, 200μm, 20 cm × 20 cm) and column chromatography was carried out on silica gel 60 (Merck, 230 −400 mesh ASTM). High-

resolution mass spectrometry analysis was carried out on an Agilent LC−UV−TOF mass spectrometer at the Mass Spectrometry facility of the Institute of Chemical Biology and Drug Discovery, Stony Brook University.

Chemical Synthesis of PEX-9 Inhibitor Compounds and Characterization Data:

***N*-(4-Difluoromethoxyphenyl)-2-(4-oxo-6-propyl-1,4-dihydropyrimidin-2-ylthio)acetamide (1a).** To a solution of bromoacetic acid (170 mg, 1.25 mmol) and EDC·HCl (239 mg, 1.25 mmol) in dichloromethane (6 mL) was added aniline (**5a**, 200 mg, 1.25 mmol) and stirred at room temperature overnight. After the completion of the reaction, the reaction mixture was diluted with dichloromethane and washed twice with 1 N hydrochloric acid, twice with saturated solution of sodium bicarbonate and twice with brine. The organic layers were collected, dried over magnesium sulfate, filtered and concentrated to afford an off-white crude product. The crude product was recrystallized from hexanes/dichloromethane to give bromoacetanilide **6a** as white solid (227 mg, 65 % yield): ^{1}H NMR (300 MHz, CDCl3) δ 4.27 (s, 2 H), 6.30-6.79 (s, 1 H), 7.21 (d, 2 H, *J* = 9Hz), 7.63 (d, 2 H, *J* = 9Hz).

To a solution of sodium hydroxide (7.2 mg, 0.18 mmol) in water (2 mL) was added 2-hydrosulfanyl-4-oxo-6-propyl-1,4-dihydropyrimidine (**7**) (30 mg, 0.18 mmol) and the mixture was stirred till all of **1** were dissolved. To the mixture was added a solution of **6a** (50 mg, 0.18 mmol) in tetrahydrofuran (2 mL) and heated at 60 °C for 2 h and then at 70 °C overnight. After the completion of reaction white precipitate was observed which was collected on a filter and recrystallized from ethanol to afford **1a** as white solid (42 mg, 63 % yield): mp. 180 ^{o}C (decomp.); ^{1}H NMR (700 MHz, DMSO-d_6) δ 0.73 (t, *J* = 7.0 Hz, 3H), 1.51 (m, 2H), 2.32 (t, *J* = 7.0 Hz, 2H), 4.05 (s, 2H), 5.97 (s, 1H), 6.97–7.29 (m, 3H), 7.62 (d, *J* = 8.4 Hz, 2H), 10.44 (s, 1H); ^{13}C NMR (175 MHz, DMSO-d_6) δ 13.4, 20.6, 35.1, 38.2, 116.5.0 (t, *J* = 256.0 Hz), 119.5, 120.4, 136.4, 146.3, 165.9; ^{19}F NMR (376 MHz, DMSO-d_6) δ -81.6; HRMS (ESI+) calcd for $C_{16}H_{18}F_2N_3O_3S$ $[M + H]^+$ 370.1031, found 370.1039 (Δ= -2.02 ppm).

In the same manner, **1b** and **1c** were synthesized.

2-(4-Oxo-6-propyl-1,4-dihydropyrimidin-2-ylthio)-N-phenylacetamide (1b). White solid; 35% yield; mp. 170 ^{o}C (decomposed); ^{1}H NMR (700 MHz, DMSO-d_6) δ ^{1}H NMR (700 MHz, DMSO-d_6) δ 0.83 (t, J = 7.0Hz, 3H), 1.46 - 1.56 (m, 2H), 2.31 (t, J = 7.0Hz, 2H), 4.04 (s, 2H), 5.90 (s, 1H), 7.04 (t, J = 7.7Hz, 1H), 7.30 (t, J = 7.7Hz, 2H), 7.56 (t, J = 7.7Hz, 2H), 10.33 (s, 1H), 12.67 (s, 1H). ^{13}C NMR (175 MHz, DMSO-d_6) δ 13.4, 20.5, 35.1, 38.5, 119.0, 123.3, 128.7, 139.0, 165.9; HRMS (ESI+) calcd for $C_{15}H_{18}N_3O_2S$ $[M + H]^+$ 304.1114, found 304.1113 (Δ= 0.29 ppm).

***N*-(4-Fluorophenyl)-2-(4-oxo-6-propyl-1,4-dihydropyrimidin-2-ylthio)acetamide (1c).** White solid; 69 % yield; mp. 191-194 ^{o}C; ^{1}H NMR (500 MHz, DMSO-d_6) δ 0.73 (t, J = 7.0 Hz, 3H), 1.45 - 1.56 (m, 2H), 2.31 (t, J = 7.0Hz, 2H), 4.02 (s, 2H), 6.94 (s, 1H), 7.10 - 7.19 (m, 2H), 7.55 - 7.62 (m, 2H), 10.30 (s, 1H), 12.54 (s,1H). ^{13}C NMR (500 MHz, DMSO-d_6) δ 13.4, 20.5, 35.0, 38.5, 115.3 (d, J = 22.1Hz), 120.7 (d, J = 7.7Hz), 135.5 (d, J = 2.5Hz), 158.0 (d, J = 238.4Hz), 165.8; ^{19}F NMR (376 MHz, DMSO-d_6) δ -119.3; HRMS (ESI+) calcd for $C_{15}H_{17}FN_3O_2S$ $[M + H]^+$ 322.1020, found 322.1020 (Δ= -0.03 ppm).

***N*-(1H-benzo[d]imidazol-2-yl)-2-(4-oxo-6-propyl-1,4-dihydropyrimidin-2-ylthio)acetamide (1d).** To a solution of thiouracil **7** (1.70 g, 10.0 mmol) and potassium carbonate (2.07 g, 15.0 mmol) in MeOH (10 mL) and water (20 mL) was added ethyl 2-bromoacetate (1.42 g, 8.5 mmol). The mixture was stirred at room temperature for 15 min and 50 mL water was added. Then, the reaction mixture was extracted with ethyl acetate (5 × 80 mL). The organic layers were combined and washed with water (100 mL) and brine (100 mL), dried over $MgSO_4$, and the solvent was removed by rotary evaporator. The crude product was purified by flash column chromatography on silica gel using MeOH/DCM as eluent to give ethyl 2-(4-oxo-6-propyl-1,4-dihydropyrimidin-2-ylthio)acetate as white solid (1.7 g, 67% yield): mp. 117-118 ^{o}C; ^{1}H NMR (300 MHz, $CDCl_3$) δ 0.93 (t, J = 7.2 Hz, 3H), 1.27 (t, J = 7.2 Hz, 3H), 1.59

– 1.65 (m, 2H), 2.43 (t, *J* = 7.2 Hz, 2H), 3.93 (s, 2H), 4.20 (q, *J* = 7.2 Hz, 2H), 6.05 (s, 1H), 13.17 (s, 1H). ^{13}C NMR (175 MHz, $CDCl_3$) δ 13.6, 14.1, 20.8, 32.8, 39.5, 61.9, 108.2, 158.9, 165.5, 168.2, 169.2; HRMS (ESI+) calcd for $C_{11}H_{17}N_2O_3S$ $[M + H]^+$ 257.0954, found 257.0953 (Δ= 0.48 ppm).

To a solution of ethyl 2-((4-oxo-6-propyl-1,4-dihydropyrimidin-2-yl)thio)acetate (1.20 g, 4.68 mmol) in MeOH and water was added lithium hydroxide (0.2 g, 9.36 mmol). The mixture was stirred at room temperature for 2 days. The reaction mixture was adjusted to pH 1 by 1N hydrochloric acid, and extracted with ethyl acetate (5 × 80 mL). The organic layers were combined and dried over $MgSO_4$, and the solvent was removed by rotary evaporator to afford thioacetic acid **8** (0.30 g, 28%) as white solid: mp. 154-155 ^{o}C; ^{1}H NMR (700 MHz, DMSO-d_6) δ 0.86 (t, *J* = 7.0 Hz, 3H), 1.56 (m, 2H), 2.30 (t, *J* = 7.0 Hz, 2H), 3.47 (s, 2H), 5.79 (s, 1H). ^{13}C NMR (175 MHz, DMSO-d_6) δ 13.6, 20.7, 36.1, 38.2, 107.4, 163.7, 164.3, 166.3, 171.2; HRMS (ESI+) calcd for $C_9H_{13}N_2O_3S$ $[M + H]^+$ 229.0641, found 229.0644 (Δ= -1.11 ppm).

To a mixture of 2-(6-oxo-4-propyl-1,6-dihydropyrimidin-2-ylthio)acetic acid (**8**) (228 mg, 1.0 mmol), 1H-benzo[d]imidazol-2-amine (**5d**, 146 mg, 1.1 mmol) and DMAP (134 mg, 1.1 mmol) in DMF (3 mL) was added EDC·HCl (211 mg, 1.1 mmol), and the mixture was stirred at RT for 24 h. 50 mL water was added, and the resulting precipitate was filtered to give a solid, which was recrystallized from 1,4-dioxane to give compound **1d** (136 mg, 40 %) as off-white solid: mp. 217 ^{o}C (decomposed); ^{1}H NMR (700 MHz, DMSO-d_6) δ 0.63 (t, *J* = 7.0 Hz, 3H), 1.50 – 1.40 (m, 2H), 2.27 (t, *J* = 7.0 Hz, 2H), 4.14 (s, 2H), 5.93 (s, 1H), 7.05-7.09 (m, 2H), 7.40-7.43 (m, 2H), 12.10 (s, 3H); ^{13}C NMR (175 MHz, DMSO-d_6) δ 13.3, 20.5, 34.5, 38.4, 106.5, 111.5, 114.1, 120.3, 121.0, 136.3, 146.7, 161.6, 162.3, 163.9, 167.7; HRMS (ESI+) calcd for $C_{16}H_{18}N_5O_2S$ $[M + H]^+$ 344.1176, found 344.118 (Δ= -1.1 ppm).

***N*-(4-Difluoromethoxyphenyl)-4-(4-oxo-6-propyl-1,4-dihydropyrimidin-2-ylthio)butanamide (2a).** To a solution of thiouracil **7** (0.85 g, 5 mmol) and potassium

carbonate (1.03g, 7.5 mmol) in methanol (5 mL) and water (10 mL) was added methyl 4-bromobutanoate (1.36g, 7.5 mmol). The solution was heated to reflux overnight. The reaction mixture was cooled to room temperature, 50 mL water was added, and the mixture was extracted with ethyl acetate (3 × 50 mL). The organic layers were combined and washed with water (50 mL) and brine (50 mL), dried over $MgSO_4$, the solvent was removed by rotary evaporator. The crude product was purified by flash column chromatography on silica gel using MeOH/DCM as eluent to give methyl 4-(4-oxo-6-propyl-1,4-dihydropyrimidin-2-ylthio)butanoate as white solid (0.64 g, 47% yield): mp. 129-130 ^{o}C; ^{1}H NMR (500 MHz, $CDCl_3$) δ 0.95 (t, *J* = 7.0 Hz, 3H), 1.64-1.71(m, 2H), 2.06 (m, 2H), 2.46 (m, 4H), 3.24 (t, *J* = 7.0 Hz, 2H) , 3.68 (s, 3H) , 6.04 (s, 1H), 12.99 (s, 1H); ^{13}C NMR (125 MHz, $CDCl_3$) δ 13.8, 21.0, 24.7, 29.9, 32.7, 39.7, 51.8, 108.0, 160.2, 165.6, 169.5, 173.4; HRMS (ESI+) calcd for $C_{12}H_{19}N_2O_3S$ $[M + H]^+$ 271.1111, found 271.111(Δ= 0.51ppm).

To a solution of methyl 4-(4-oxo-6-propyl-1,4-dihydropyrimidin-2-ylthio)butanoate (500 mg, 1.84 mmol) in MeOH and water was added lithium hydroxide (88.1 mg, 3.68 mmol), and the mixture was stirred at room temperature for 2 days. The mixture was adjusted to pH 1 by 1N hydrochloric acid to form white precipitate. The precipitate was collected on a filter to afford 4-(4-oxo-6-propyl-1,4-dihydropyrimidin-2-ylthio)butanoic acid **9** as white solid (308.0 mg, 66% yield): mp. 139-141 ^{o}C; ^{1}H NMR (300 MHz, $CDCl_3$) δ 0.95 (t, *J* = 7.3 Hz, 3H), 1.68 (m, 2H), 2.01-2.14(m, 2H), 2.49 (m, 4H), 3.28 (t, *J* = 6.5 Hz, 2H), 6.04 (s, 1H); ^{13}C NMR (175 MHz, $CDCl_3$) δ 13.8, 21.1, 24.5, 29.9, 32.8, 39.7, 107.7, 160.3, 165.9, 170.2, 178.5; HRMS (ESI+) calcd for $C_{11}H_{17}N_2O_3S$ $[M + H]^+$ 257.0954, found 257.0958(Δ= -1.33ppm).

To a mixture of **9** (190 mg, 0.74 mmol), 4-(difluoromethoxy)aniline (**5a,** 130.5 mg, 0.82 mmol) and 4-(dimethylamino)pyridine (DMAP) (99.4 mg, 0.81 mmol) in dimethylformamide (DMF) (3 mL) was added *N'*-ethylcarbodiimide hydrochloride (EDC·HCl (156 mg, 0.81 mmol), the mixture was stirred at room temperature for 1 h. Then, 100 mL water was added to the

reaction mixture to form off-white precipitate, which was collected on a filter to give an off-white solid. The solid was dissolved in ethyl acetate and dried over $MgSO_4$, filtered, and the solvent was removed by rotary evaporator. The crude product was purified by recrystallization from ethyl acetate/hexane to afford **2a** as white solid (120.4 mg, 41% yield): mp. 174-177 ^oC; ^1H NMR (500 MHz, $CDCl_3$) δ 0.92 (t, *J* = 7.5 Hz, 3H), 1.64 (m, 2H), 2.06 – 2.22 (m, 2H), 2.42 (t, *J* = 7.5 Hz, 2H), 2.49 (t, *J* = 6.9 Hz, 2H), 3.31 (t, *J* = 5.7 Hz, 2H), 6.01 (s, 1H), 6.45 (t, *J* = 74.0 Hz, 1H), 7.07 (d, *J* = 8.6 Hz, 2H), 7.55 (d, *J* = 8.6 Hz, 2H), 7.92 (s, 1H), 12.69 (s, 1H). ^{13}C NMR (125 MHz, $CDCl_3$) δ 13.8, 21.1, 24.8, 30.2, 35.5, 39.7, 107.8, 116.1(t, *J* = 259 Hz), 120.6, 121.3, 135.6, 147.3, 160.2, 165.5, 169.9, 170.5; ^{19}F NMR (376 MHz, $CDCl_3$) δ -80.7; HRMS (ESI+) calcd for $C_{18}H_{22}F_2N_3O_3S$ $[M + H]^+$ 398.1344, found 398.1345 (Δ = -0.03 ppm).

In the same manner, compound **2c** was synthesized.

***N*-(4-Fluorophenyl)-4-(4-oxo-6-propyl-1,4-dihydropyrimidin-2-ylthio)butanamide (2c).** White solid; 39% yield. mp. 180-182 ^oC; ^1H NMR (300 MHz, $CDCl_3$) δ 0.83-0.96 (t, *J* = 7.3 Hz, 3H), 1.57-1.69 (m, 2H), 2.05-2.21 (m, 2H), 2.33-2.55 (m, 4H), 3.31 (t, *J* = 6.3 Hz, 2H), 6.02 (s, 1H), 7.00 (t, *J* = 8.7 Hz, 2H), 7.49 (m, 2H), 7.64 (s, 1H), 12.45 (s, 1H). ^{13}C NMR (175 MHz, DMSO-d_6) δ 13.4, 20.5, 24.8, 29.2, 34.9, 38.5, 115.2 (d, *J* = 22.0Hz), 120.7 (d, *J* = 7.7Hz), 135.7 (d, *J* = 2.3Hz), 157.1, 158.5, 170.3; ^{19}F NMR (376 MHz, $CDCl_3$) δ -119.7; HRMS (ESI+) calcd for $C_{17}H_{21}FN_3O_2S$ $[M + H]^+$ 350.1333, found 350.134 (Δ = -2.12ppm).

4-(4-Oxo-3,4,5,6,7,8-hexahydroquinazolin-2-ylthio)-N-phenylbutanamide (3b). Ethyl 2-oxocyclohexane-1-carboxylate 10 (1.70 g, 10.0 mmol) and thiourea (1.52 g, 20.0 mmol) were added to a sodium methoxide solution (0.58 g sodium in 20 mL methanol), and the mixture was refluxed overnight. The solvent was removed and the residue was dissolved in hot water (50 mL). Glacial acetic acid (6 mL) was added dropwise to make the solution acidic until a white solid was formed. The precipitate was collected by a filter and washed successively with saturated sodium bicarbonate (3 × 10 mL) and water (3 × 10 mL), and recrystallized from ethyl

acetate (30 mL) to afford 2-sulfhydryl-5,6,7,8-tetrahydroquinazolin-4(3H)-one (**11**) (1.70 g, 93%) as white solid: mp. > 230 ^{o}C; 1H NMR (700 MHz, DMSO-d6) δ 1.53-1.76 (m, 4H), 2.16 (t, J = 6.0 Hz, 2H), 2.36 (t, J = 6.0 Hz, 2H), 12.09 (s, 1H), 12.25 (s, 1 H); 13C NMR (175 MHz, DMSO-d6) δ 20.5, 20.7, 20.9, 25.5, 111.6, 149.5, 161.3, 173.9; HRMS (ESI+) calcd for C8H11N2OS [M + H]+ 183.0587, found 183.0587 (Δ= -0.44 ppm).

To a solution of **11** (1.59 g, 8.72 mmol) in anhydrous methanol (15 mL) was added methyl 4-bromobutanoate (1.72 g, 9.55 mmol) and potassium carbonate (1.31 g, 9.48 mmol). The reaction mixture was heated to reflux for overnight. After cooled to room temperature, the reaction mixture was concentrated in vacuo to remove the solvent. To the residue water (50 mL) was added, and extracted with dichloromethane (4 $\times$ 40 mL). The combined organic phases were washed with brine (5 mL), dried over $MgSO_4$, and concentrated in vacuo to give a crude product, which was purified by recrystallization from ethyl acetate to afford methyl 4-(4-oxo-3,4,5,6,7,8-hexahydroquinazolin-2-ylthio)butanoate (1.80 g, 73%) as white solid: mp. 149 – 150 °C; ^{1}H NMR (700 MHz, $CDCl_3$) δ 1.69 - 1.79 (m, 4H), 2.01 - 2.06 (m, 2H), 2.47 (m, 4H), 2.59 (t, *J* = 7.0 Hz, 2H), 3.22 (t, *J* = 7.0 Hz, 2H), 3.67 (s, 3H); ^{13}C NMR (175 MHz, $CDCl_3$) δ 21.7, 21.8, 22.2, 24.7, 29.8, 31.6, 32.7, 51.8, 117.6, 156.4, 162.0, 165.0, 173.5; HRMS (ESI+) calcd for $C_{13}H_{19}N_2O_3S$ $[M + H]^+$ 283.1111, found 283.1117 (Δ = -2.09 ppm).

To a mixture of 2 N sodium hydroxide (1.51 g in 19 mL water) and ethanol (22 mL) was added methyl 4-(4-oxo-3,4,5,6,7,8-hexahydroquinazolin-2-ylthio)butanoate (1.34 g, 4.75 mmol) at room temperature. The mixture was stirred for overnight at room temperature. The reaction mixture was adjusted to pH 5 with 1N hydrochloric acid, and extracted with dichloromethane (5 $\times$ 40 mL). The combined organic phases were dried over $MgSO_4$, and concentrated in vacuo to give a residue, which was recrystallized from dichloromethane to afford 4-(4-oxo-3,4,5,6,7,8-hexahydroquinazolin-2-ylthio)butanoic acid **12** (1.26 g, 99% yield) as white solid: mp. 176 –

177 °C; ^{1}H NMR (700 MHz, CD_3OD) δ 1.71 - 1.81 (m, 4H), 1.96 - 2.03 (m, 2H), 2.39 (t, *J* = 6.3 Hz, 2H), 2.43 (t, *J* = 7.0 Hz, 2H), 2.57 (t, *J* = 6.3 Hz, 2H), 3.23 (t, *J* = 7.0 Hz, 2H); ^{13}C NMR (175 MHz, CD_3OD) δ 22.7, 22.9, 23.1, 26.0, 30.4, 33.4, 176.6; HRMS (ESI+) calcd for $C_{12}H_{17}N_2O_3S$ $[M + H]^+$ 269.0954, found 269.0959 (Δ= -1.54 ppm).

To a mixture of thiobutanoic acid **12** (134 mg, 0.50 mmol), aniline **5b** (70 mg, 0.75 mmol) and DMAP (67 mg, 0.55 mmol) in DMF (2 mL) was added EDC·HCl (105 mg, 0.55 mmol), and the mixture was stirred at room temperature for 48 h. To the reaction mixture 50 mL water was added with stirring to form precipitate. The resulting precipitate was collected on a filter and recrystallized from ethyl acetate to give **3b** (79 mg, 46% yield) as an off-white solid: mp. 193-194 °C; ^{1}H NMR (500 MHz, DMSO-d_6) δ 1.56 - 1.67 (m, 4H), 1.91 - 1.97 (m, 2H), 2.26 (m, 2H), 2.39 - 2.45 (m, 4H), 3.16 (t, *J* = 7.0 Hz, 2H), 7.01 (t, *J* = 8.0 Hz, 1H), 7.27 (t, *J* = 8.0 Hz, 2H), 7.58 (d, *J* = 8.0 Hz, 2H), 9.90 (s, 1H), 12.42 (s, 1H); ^{13}C NMR (125 MHz, DMSO-d_6) δ 21.4, 21.8, 24.7, 29.0, 31.1, 34.9, 119.0, 122.9, 128.6, 139.3, 170.3; HRMS (ESI+) Calcd for $C_{18}H_{22}N_3O_2S$ $[M + H]^+$ 344.1427, found 344.1430 (Δ= -0.71 ppm).

In the same manner, compounds **3a, 3c, and 3d** were synthesized.

***N*-(4-Difluoromethoxyphenyl)-4-(4-oxo-3,4,5,6,7,8-hexahydroquinazolin-2-ylthio)butanamide (3a).** Off-white solid; 52% yield; mp. 197-198 °C; ^{1}H NMR (700 MHz, Acetone-d_6) δ 1.63-1.73 (m, 4H), 2.09 (m, 2H), 2.35 (t, *J* = 6.3 Hz, 2H), 2.47 (t, *J* = 6.3 Hz, 2H), 2.53 (t, *J* = 7.0 Hz, 2H), 3.27 (t, *J* = 7.0 Hz, 2H), 6.90 (t, *J* = 74.4 Hz, 1H), 7.11 (d, *J* = 8.4 Hz, 2H), 7.70 (d, *J* = 8.4 Hz, 2H), 9.27 (s, 1H), 11.46 (s, 1H); ^{13}C NMR (175 MHz, Acetone-d_6) δ 22.4, 22.5, 23.0, 26.0, 32.2, 35.9, 117.6 (t, *J* =255.5 Hz), 117.9, 120.6, 121.3, 137.9, 147.6 (t, *J* =2.6 Hz), 157.2, 161.2, 163.4, 171.2; ^{19}F NMR (376 MHz, Acetone-d_6) δ -82.3; HRMS (ESI+) Calcd for $C_{19}H_{22}F_2N_3O_3S$$[M + H]^+$ 410.1344, found 410.1346 (Δ= -0.33 ppm).

***N*-(4-Fluorophenyl)-4-(4-oxo-3,4,5,6,7,8-hexahydroquinazolin-2-ylthio)butanamide (3c).** White solid; 70% yield; mp. 211.5 – 213 °C; ^{1}H NMR (700 MHz, DMSO-d_6) δ 1.56 - 1.66

(m, 4H), 1.94 (m, 2H), 2.26 (t, *J* = 5.6 Hz, 2H), 2.41 (t, *J* = 7.0 Hz, 4H), 3.15 (t, *J* = 7.0 Hz, 2H), 7.10 - 7.14 (m, 2H), 7.57 - 7.61 (m, 2H), 9.96 (s, 1H), 12.44 (s, 1H); ^{13}C NMR (175 MHz, DMSO-d_6) δ 21.4, 21.8, 24.7, 29.0, 31.1, 34.8, 115.2 (d, *J* = 21.9 Hz),120.7 (d, *J* = 7.7 Hz), 135.7 (d, *J* = 2.3Hz), 157.8 (d, *J* = 238Hz), 170.3; ^{19}F NMR (376 MHz, DMSO-d_6) δ -119.8; HRMS (ESI+) calcd for $C_{18}H_{21}FN_3O_2S$ $[M + H]^+$ 362.1333, found, 362.1337 (Δ= -1.05 ppm).

***N*-(1H-Benzo[d]imidazol-2-yl)-4-(4-oxo-3,4,5,6,7,8-hexahydroquinazolin-2-ylthio)butanamide (3d).** Off-white solid; 22% yield; mp. > 230 ^{o}C; ^{1}H NMR (700 MHz, DMSO-d_6) δ 1.55 - 1.66 (m, 4H), 2.09 (m, 2H), 2.21 - 2.27 (m, 2H), 2.35 - 2.41 (m, 2H), 3.21 (t, *J* = 5.6 Hz, 2H), 3.27 (t, *J* = 5.6 Hz, 2H), 6.93 (t, *J* = 7.0 Hz, 1H), 7.11 - 7.22 (m, 2H), 7.38-7.48 (m, 3H), 12.45 (s, 1H); ^{13}C NMR (125 MHz, DMSO-d_6)) δ 21.4, 21.8, 23.7, 28.5, 31.0, 36.2, 113.6, 115.7, 116.4, 119.5, 124.1, 130.0, 143.4, 154.6, 156.5, 160.0, 162.4, 173.8; HRMS (ESI+) Calcd for $C_{19}H_{22}N_5O_2S[M + H]^+$ 384.1489, found 384.1494 (Δ= -1.45 ppm).

4-(4-Oxo-3,4-dihydroquinazolin-2-ylthio)-*N*-phenylbutanamide (4b). A mixture of 2-sulfhydrylquinazolin-4(3H)-one (**13**) (1.78 g, 10.0 mmol), methyl 4-bromobutanoate (2.72 g, 15.0 mmol) and K_2CO_3 (2.07 g, 15.0 mmol) in methanol (10 mL) and water (20 mL) was refluxed for 1 h. After cooled to room temperature, 50 mL water was added and the reaction mixture was extracted with ethyl acetate (3 × 50 mL). The combined organic layers were washed with (50 mL) and brine (50 mL), dried over $MgSO_4$, and concentrated in vacuo to give a crude product, which was purified by recrystallization from ethyl acetate/hexanes to give methyl 4-(4-oxo-3,4-dihydroquinazolin-2-ylthio)butanoate (2.24 g, 81% yield) as white solid: mp. 153-154 ^{o}C; ^{1}H NMR (700 MHz, DMSO-d_6) δ 1.96 (m, 2H), 2.45 (t, *J* = 7.0 Hz, 2H) , 3.23 (t, *J* = 7.0 Hz, 2H) , 3.58 (s, 3H), 7.39 (t, *J* = 7.0 Hz, 1H), 7.49 (d, *J* = 7.0 Hz, 1H) , 7.73 (t, *J* = 7.0 Hz, 1H) , 8.02 (d, *J* = 7.0 Hz, 1H), 12.55 (s, 1H). ^{13}C NMR (175 MHz, DMSO-d_6) δ 24.3, 28.9, 32.1, 51.4, 120.0, 125.6, 125.9, 126.0, 134.5, 148.3, 155.5, 161.3, 172.8. HRMS (ESI+) Calcd for $C_{13}H_{15}N_2O_3S$ $[M + H]^+$ 279.0798, found 279.0802 (Δ= -1.42 ppm).

A mixture of methyl 4-(4-oxo-3,4-dihydroquinazolin-2-ylthio)butanoate (1.39 g, 5.0 mmol) in DMSO (1mL) and LiOH (aqueous, 1M, 10 mL) was stirred at room temperature for 2 h. To the reaction mixture was added 100 mL water and adjusted to pH 1. The resulting precipitate was collected on a filter, and washed with water to give 4-(4-oxo-3,4-dihydroquinazolin-2-ylthio)butanoic acid (**14**) (1.14 g, 86% yield) as white solid: mp. 178-179 ^{o}C; ^{1}H NMR (500 MHz, DMSO-d_6) δ 1.90 – 1.96 (m, 2H), 2.37 (t, J = 7.0 Hz, 2H), 3.24 (t, J = 7.0 Hz, 2H), 7.41 (t, J = 7.5 Hz, 1H), 7.52 (d, J = 7.5 Hz, 1H), 7.75 (t, J = 7.5 Hz, 1H), 8.02 (d, J = 7.5 Hz, 1H), 12.37 (s, 2H). ^{13}C NMR (175 MHz, DMSO-d_6) δ 24.3, 29.1, 32.5, 120.0, 125.6, 125.9, 126.0, 134.6, 148.3, 155.6, 161.3,173.9; HRMS (ESI+) Calcd for $C_{12}H_{13}N_2O_3S$ [M + H] $^{+}$ 265.0641, found: 265.0646 (Δ= -1.56 ppm).

To a mixture of 4-(4-oxo-3,4-dihydroquinazolin-2-ylthio)butanoic acid (**14**) (132 mg, 0.50 mmol), aniline (186 mg, 2.0 mmol) and DMAP (67 mg, 0.55 mmol) in DMF (2 mL) was added EDC·HCl (144 mg, 0.75 mmol), and the mixture was stirred at room temperature for 18 h. To the reaction mixture was added 20 mL water with stirring. The resulting precipitate was collected on a filter and recrystallized from 1,4-dioxane to give **4b** (61 mg, 36% yield) as white solid: mp. > 230 ^{o}C; ^{1}H NMR (700 MHz, DMSO-d_6) δ 1.56 – 1.60 (m, 2H), 2.03 (t, J = 7.0 Hz, 2H), 2.84 (t, J = 7.0 Hz, 2H), 6.57 (t, J = 7.0 Hz, 1H), 6.83 (t, J = 7.0 Hz, 2H), 6.95 (t, J = 7.0 Hz, 1H), 7.01 (d, J = 8.4 Hz, 1H), 7.13 (d, J = 7.0 Hz, 2H), 7.25 (t, J = 7.0 Hz, 1H) , 7.57 (d, J = 7.0 Hz, 1H), 9.48 (s, 1H), 12.12 (s, 1H); ^{13}C NMR (175 MHz, DMSO-d_6) δ 24.8, 29.2, 35.1, 119.0, 112.0, 123.0, 125.6, 126.0, 128.6, 134.5, 139.3, 148.4, 155.6, 161.2, 170.4. HRMS (ESI+) Calcd for $C_{18}H_{18}N_3O_2S$ [M + H] $^{+}$ 340.1114, found: 340.1121 (Δ= -2.0 ppm).

In the same manner, compounds **4a, 4c, and 4d** were synthesized.

***N*-(4-(Difluoromethoxy)phenyl)-4-(4-oxo-3,4-dihydroquinazolin-2-ylthio)butanamide (4a).** Off-white solid; 42% yield; mp. 210-211 ^{o}C. ^{1}H NMR (700 MHz, Acetone-d_6) δ 2.13 - 2.23(m, 2H), 2.59 (t, J = 7.0 Hz, 2H), 3.41 (t, J = 7.0 Hz, 2H), 6.90 (t, J =

74.2 Hz, 1H), 7.11 (d, *J* = 8.4 Hz, 2H), 7.40 (t, *J* = 7.7 Hz, 1H), 7.49 (d, *J* = 7.7 Hz, 1H), 7.69 (m, 3H), 8.09 (d, J = 7.7 Hz, 1H), 9.25 (s, 1H), 11.22 (s, 1H); ^{13}C NMR (175 MHz, DMSO-d_6) δ 24.7, 29.2, 34.9, 116.5 (t, *J* = 256 Hz), 119.5, 120.0, 120.4, 125.6, 126.0, 134.5, 136.7, 146.1, 148.40, 155.6, 161.3, 170.4; ^{19}F NMR (376 MHz, DMSO-d_6) δ -81.4; HRMS (ESI+) Calcd for $C_{19}H_{18}F_2N_3O_3S$ [M + H] $^+$ 406.1031, found 406.1033 (Δ = -0.44 ppm).

***N*-(4-Fluorophenyl)-4-((4-oxo-3,4-dihydroquinazolin-2-yl)thio)butanamide (4c).** White solid; 46% yield; mp. 216-217 ^{o}C; ^{1}H NMR (500 MHz, DMSO-d_6) δ 1.20 - 2.05 (m, 2H), 2.47 (t, *J* = 7.0 Hz, 2H), 3.29 (t, *J* = 7.0 Hz, 2H), 7.09 - 7.14 (m, 2H), 7.38-7.41 (m, 1H), 7.45 (d, *J* = 8.0 Hz, 1H), 7.57-7.60 (m, 2H), 7.68 – 7.72 (m, 1H), 8.02 (dd, *J* = 8.0, 1.5 Hz, 1H), 9.97 (s, 1H), 12.56 (s, 1H). ^{13}C NMR (125 MHz, DMSO-d_6) δ 24.7, 29.2, 34.9, 115.2 (d, *J* = 21.9 Hz), 112.0, 120.7 (d, *J* = 7.7 Hz), 125.6, 126.0, 126.0, 134.5, 135.7 (d, *J* = 2.4 Hz), 148.4, 155.5, 157.8 (d, *J* = 237.9 Hz), 161.2, 170.3; ^{19}F NMR (376 MHz, DMSO-d_6) δ -119.8; HRMS (ESI+) Calcd for $C_{18}H_{17}FN_3O_2S$ [M + H] $^+$ 358.1020, found: 358.1027 (Δ= -1.99 ppm).

***N*-(1H-Benzo[d]imidazol-2-yl)-4-(4-oxo-3,4-dihydroquinazolin-2-ylthio)butanamide (4d).** A white solid; 25% yield; mp. > 230 ^{o}C; ^{1}H NMR (700 MHz, DMSO-d_6) δ 2.05-2.09 (m, 2H), 2.61 (t, *J* = 7.0 Hz, 2H), 3.31 (t, *J* = 7.0 Hz, 2H), 7.07 (m, 2H), 7.33 - 7.50 (m, 4H), 7.58 (t, *J* = 7.0 Hz, 1H), 8.00 (d, *J* = 7.0 Hz, 1H), 11.52 (s, 1H), 12.06 (s, 1H), 12.57 (s, 1H); ^{13}C NMR (175 MHz, DMSO-d_6) δ 24.5, 29.0, 31.1, 111.5, 116.9, 120.0, 121.8, 125.5, 126.0, 132.5, 134.4, 140.5, 146.6, 148.4, 155.6, 161.3, 171.8; HRMS (ESI+) Calcd for $C_{19}H_{17}N_5O_2S$ [M + H] $^+$ 380.1176, found 380.1178 (Δ = - 0.54 ppm).

***N*-Hexyl-4-(4-oxo-3,4-dihydroquinazolin-2-ylthio)butanamide (4e).** To a mixture of 4-(4-oxo-3,4-dihydroquinazolin-2-ylthio)butanoic acid (**14**) (79 mg, 0.30 mmol) in 1,4-dioxane (2 mL) was added carbonyldiimidazole (CDI) (73 mg, 0.45 mmol), and the mixture was stirred at room temperature for 1h. 1-Hexylamine (**5e**, 61 mg, 0.60 mmol) and DMF (5mL) were added to the mixture and heated at 60 ^{o}C for 48 h. After cooled to room temperature, 40 mL water was

added, and the reaction mixture was extracted with EtOAc (3 × 20 mL). The combined organic layers were washed with water (20 mL) and brine (20 mL), dried over $MgSO_4$, and concentrated in vacuo to give a yellow oil. Then, 20 mL hexane was added to this oil with stirring to form precipitate. The resulting precipitate was collected on a filter to give **4e** (46.7 mg, 45% yield) as white solid: mp. 168-169 ^{o}C. ^{1}H NMR (700 MHz, DMSO-d_6) δ 0.81 (t, J = 5.6 Hz, 3H), 1.20 (m, 6H), 1.35 (m, 2H), 1.92 (m, 2H), 2.22 (t, J = 7.0 Hz, 2H), 3.01 (m, 2H), 3.20 (t, J = 7.0 Hz, 2H), 7.40 (t, J = 7.7 Hz, 1H), 7.49 (d, J = 7.7 Hz, 1H), 7.73 (t, J = 7.7 Hz, 1H), 7.82 (s, 1H), 8.02 (d, J = 7.7 Hz, 1H), 12.55 (s, 1H); ^{13}C NMR (175 MHz, DMSO-d_6) δ 13.9, 22.1, 25.0, 26.1, 29.1, 29.3, 31.0, 34.2, 38.5, 120.0, 125.5, 125.9, 126.0, 134.5, 148.4, 155.7, 161.3, 171.0; HRMS (ESI+) Calcd for $C_{18}H_{26}N_3O_2S$ [M + H] $^{+}$ 348.1740, found 348.1742 (Δ= -0.54 ppm).

Cell Culture and Transfection. COS-1 monkey epithelial, human fibrosarcoma HT-1080 and breast MCF-7 cancer cell lines were purchased from American Type Culture Collection (ATCC) and were maintained in Dulbecco's modified Eagle medium (DMEM; Invitrogen) containing 10% fetal calf serum under 5% CO_2 atmosphere. Transfection of plasmid DNA (human) into cells was achieved using polyethylenimine (Polysciences) and the transfected cells were incubated for 48 hours at 37 °C followed by biochemical and biologic assays unless otherwise stated.

Two-Dimensional Dot Migration Assay. Transfected cells were mixed with an equal volume of neutralized type I collagen (3 mg/mL) on ice. The cell–collagen mixture (1 μL of 1 × 10^7 cell/mL) was then dotted onto a 96-well plate. After solidification of cell–collagen dots, the cell–collagen hemispheres were covered with 100 μL of complete media and incubated for 8 - 18 hours (incubation time varies by cell type), followed by staining with DAPI nuclear dye and counting of the migrated cells using Nikon Elements Basic Research Software analysis tools.[50]

Co-immunoprecipitation. Twenty-four hours following transfection, the conditioned

medium in the absence of serum was collected from the transfected HT1080 cells. The cells were then lysed in RIPA buffer containing 10 mM Tris-Cl (pH 8.0), 1 mM EDTA, 1% Triton X-100, 0.1% sodium deoxycholate, 0.1% SDS, 140 mM NaCl, and protease inhibitors mixture (Sigma). Both the conditioned medium and the cell lysates were incubated with specific antibodies overnight (18 hours) at 4 °C. Antigen antibody complexes were precipitated with protein A-agarose beads followed by a brief centrifugation, washing, and then electrophoresis in a 10% SDS-polyacrylamide gel. Western blotting was then followed using a corresponding antibody as previously described.[12]

Immunofluorescence. Cultured cells were fixed with 4% paraformaldehyde/phosphate-buffered saline (PBS) followed by blocking with 5% bovine serum albumin (BSA)/PBS. Both FAK and PAX were detected with an anti-p-FAK$^{Tyr\ 576/577}$ and anti-p-PAX^{Tyr118} antibody followed by secondary antibodies conjugated with anti-rabbit Alexa 568 or Alexa 488, respectively (Invitrogen). For colocalization experiments, MMP-9 was detected with an anti-MMP-9 antibody followed by a secondary antibody conjugated with anti-rabbit Alexa 488 while $\alpha 4$ and $\beta 1$ integrins were detected with an anti-$\alpha 4$ integrin and anti-$\beta 1$ integrin respectively followed by a secondary antibody conjugated with anti-mouse Alexa 568. Nuclei were counterstained with DAPI (Invitrogen). Images were captured using a Zeiss LSM 510 META NLO Two-Photon Laser Scanning Confocal Microscope System (Central Microscopy Imaging Center, Stony Brook University).

Fluorogenic Assay of Enzyme Activity. Mca-PLGL-Dpa-AR-NH_2 fluorogenic peptide substrate (final concentration of 10 μM in DMSO) was incubated with the compounds and *p*-aminophenylmercuric acetate (APMA)-activated proMMP-9 for 30 minutes at 25 °C before detection. Fluorescence emission at 405 nm with excitation at 320 nm was measured in a fluorescent plate reader (Gemini EM; Molecular Devices).[51]

Cell Viability. HT1080 cells were cultured in complete media with or without compound

3c. Media and drugs were changed on a bi-daily basis, and cell viability was monitored by MTT assay [3-(4,5-dimethylthiazol-2-yl)-2,5-diphenyltetrazolium bromide] (Promega, Madison, WI). Each day, cells were exposed to MTT and incubated at 37 °C for 4 hours. The reaction was stopped, and formazan crystals were solubilized; the resultant solution was subject to colorimetric spectrophotometry and read at a wavelength of 570 nm.[52]

Chorioallantoic Membrane Angiogenesis and Invasion Assay. The chorioallantoic membrane (CAM) assay was performed as previously described.[53] Fertilized white chicken eggs (SPF Premium, Charles River Laboratory, North Franklin, CT) were incubated at 37 °C in 70% humidity for 3 days. The embryos were then incubated *ex ovo* in a sterile Petri dish for 7 days. Gelatin sponges adsorbed with HT1080 cells treated with or without compound **3c** were implanted on the CAM surface and neovasculature was counted on day 4 postimplantation.[54, 55] For histochemical analysis of the chorioallantoic membrane, embryos were treated as for the angiogenesis assay, except at day 10 the embryos were inoculated with pretreated HT1080 cells mixed with a type IV collagen solution (3 mg/mL). After a 7-day incubation, CAM segments containing the cell dot collagen mixture were isolated, formalin fixed and sectioned by microtome into 6-*μ*m sections after embedding in OCT. Sections were then stained with hematoxylin and counterstained with eosin.[56]

proMMP-9 Protein Purification. For purification of proMMP-2 and proMMP-9 protein, COS-1 cells stably expressing each respective MMP was incubated overnight in 10 mL of serum-free medium until 500 mL was collected for purification via a gelatin-sepharose column. Both proMMP-2 and proMMP-9 have 3 fibronectin repeats present in their gelatin binding domain which allowed us to capture and collect the secreted protein present in the serum-free medium fraction. Protein was then eluted off the gelatin sepharose column using 5% DMSO and then dialyzed to remove any organic contaminants. A coomassie blue gel was then ran to check the purity of the samples to ensure no protein contamination was present in final

solution. All methods were followed as previously described.[57]

Fluorescence Spectroscopy. Binding of compound **3c** to proMMP-9 was assayed by observing the change of tryptophan emission upon binding. Purified recombinant proMMP-9 (0.5 μM) or MMP-9/MMP-2PEX (0.5 μM) was diluted in TNC buffer (50 mM Tris-HCl pH. 7.5, 150 nM NaCl, 10 mM $CaCl_2$; pH 7.5) in the presence or absence of compound **3c**. As a control for protein stability and loss, an analogous buffer solution was added to the protein. The protein sample was excited at 280 nm and emission scans were collected from 300 to 425 nm, using slit widths of 0.3 nm on a QM-4/200SE spectrofluorimeter with double excitation and emission monochromators. Between each titration, protein/inhibitor mixture was gently stirred for 1 min at room temperature before collecting each reading. Three emission scans were collected and averaged at each concentration. The K_d was determined using the Prism software package (GraphPad V5) to fit the data to Equation: $\mathbf{\Delta F/\Delta F_{Max}}$ in which ΔF is the nm shift for a given titration and ΔF_{Max} is the maximal nm shift observed overall.

Small Molecule DOCKing. To DOCK the MMP-9 PEX domain inhibitors and predict the binding mode, the inhibitors were first created via the Advanced Chemistry Development Chemsketch software (ACD Labs, Toronto, Canada) in the MOL format. The molecules were then loaded into the program Avogadro to undergo energy minimization and were then saved as PDB format files. Once in PDB format, the molecules were individually loaded into the AutoDock Tools (The Scripps Research Institute, La Jolla, California) program and assigned charges, rotatable bonds, and a root. The molecules were saved as a pdbqt files and then used for DOCKing. The crystal structure of the PEX domain of MMP-9 was downloaded from rcsb.org (PDB code 1ITV). Chain B and all sulfate ions were deleted, followed by a brief energy minimization of the receptor via the AMBER force field. The parameters are as follows:

Steepest descent steps: 100

Steepest descent size (Angstroms): 0.01

Conjugate Gradient steps: 30

Conjugate Gradient step size (Angstroms): .02

Force Field: AMBER ff14SB (AM1-BCC)

The compounds docked underwent energy minimization via the Merck Molecular Force Field 94s (MMFF94s). DOCKing was performed via AutoDock Vina with the following parameters (untransformed coordinates of protein):

Box center (x axis) = -42.494

Box center (y axis) = -27.748

Box center (z axis) = 5.00

Box size (x axis) = 22

Box size (y axis) = 22

Box size (z axis) = 20

Exhaustiveness = 64

The results were loaded in UCSF Chimera (UCSF, San Francisco, California) and saved as JPEG images.

Statistical Analysis. Data are expressed as the mean ± standard error of triplicates. Each experiment was repeated at least three times. The Student *t* test and analysis of variants (ANOVA) were used to assess differences with *, $P < 0.05$; **, $P < 0.01$; ***, $P < 0.001$.

ASSOCIATED CONTENTS

AUTHOR INFORMATION

Corresponding Author

*Nicole S Sampson, nicole.sampson@stonybrook.edu; +1-632-632-7952 (phone); +1-631-632-5731 (Fax).

Author Contributions

J.C. and N.S.S. conceived the project. V.M.A. performed and contributed to designing all

protocols and experiments. I.O, A.K., X. R., K.K., Q.G. contributed through designing and synthesizing all PEX-9 parental and derivative compounds. M.A. contributed through performing the DOCKing analysis of all derivative compounds. M.T. and M.S. contributed through helping design and perform STD NMR experiments in addition to kinetic experiments to measure Kd values. V.M.A prepared all figures and tables. All authors contributed to writing, reviewing, commenting on, and approving the final manuscript.

Notes

The authors declare no competing financial interests.

ACKNOWLEDGEMENTS

This work was supported by NIH 1R01CA166936 (to J. Cao and N.S. Sampson) and a seed grant from the Institute of Chemical Biology and Drug Discovery (to I. Ojima). We are grateful to Weiyi Li for all her hard work and guidance in helping use the Zeiss LSM 510 META NLO Two-Photon Laser Scanning Confocal Microscope System at SBU's CMIC core facility. We also thank all members of the Cao and Sampson laboratory for insightful discussion and support given throughout the duration of this project.

SUPPORTING INFORMATION

The Supporting Information is available free of charge on the ACS Publications website at DOI: xxxxxxxxxxxxxxx

Supplemental experimental procedures, figures, data and spectra for compounds are described.

REFERENCES

1. Weigelt, B., Peterse, J. L., and van 't Veer, L. J. (2005) Breast cancer metastasis: markers and models, *Nat. Rev. Cancer 5*, 591-602.
2. Curran, S., and Murray, G. I. (1999) Matrix metalloproteinases in tumour invasion and metastasis, *J. Pathol. 189*, 300-308.
3. Curran, S., and Murray, G. I. (2000) Matrix metalloproteinases: molecular aspects of their roles in tumour invasion and metastasis, *Eur. J. Cancer 36*, 1621-1630.
4. Deryugina, E. I., and Quigley, J. P. (2006) Matrix metalloproteinases and tumor metastasis, *Cancer Metastasis Rev. 25*, 9-34.
5. Kessenbrock, K., Plaks, V., and Werb, Z. (2010) Matrix metalloproteinases: regulators of the tumor microenvironment, *Cell 141*, 52-67.
6. Coussens, L. M., Fingleton, B., and Matrisian, L. M. (2002) Matrix metalloproteinase inhibitors and cancer: trials and tribulations, *Science 295*, 2387-2392.
7. Cathcart, J., Pulkoski-Gross, A., and Cao, J. (2015) Targeting Matrix Metalloproteinases in Cancer: Bringing New Life to Old Ideas, *Genes Dis. 2*, 26-34.
8. Chou, J., Chan, M. F., and Werb, Z. (2016) Metalloproteinases: a Functional Pathway for Myeloid Cells, *Microbiol. Spectr. 4*.
9. Rodriguez, D., Morrison, C. J., and Overall, C. M. (2010) Matrix metalloproteinases: what do they not do? New substrates and biological roles identified by murine models and proteomics, *Biochim. Biophys. Acta. 1803*, 39-54.
10. Fanjul-Fernandez, M., Folgueras, A. R., Cabrera, S., and Lopez-Otin, C. (2010) Matrix metalloproteinases: evolution, gene regulation and functional analysis in mouse models, *Biochim. Biophys. Acta. 1803*, 3-19.
11. Dufour, A., Sampson, N. S., Zucker, S., and Cao, J. (2008) Role of the hemopexin domain of matrix metalloproteinases in cell migration, *J. Cell Physiol. 217*, 643-651.
12. Dufour, A., Zucker, S., Sampson, N. S., Kuscu, C., and Cao, J. (2010) Role of matrix metalloproteinase-9 dimers in cell migration: design of inhibitory peptides, *J. Biol. Chem. 285*, 35944-35956.
13. Cha, H., Kopetzki, E., Huber, R., Lanzendorfer, M., and Brandstetter, H. (2002) Structural basis of the adaptive molecular recognition by MMP9, *J. Mol. Biol. 320*, 1065-1079.
14. Sternlicht, M. D., and Werb, Z. (2001) How matrix metalloproteinases regulate cell behavior, *Annu. Rev. Cell Dev. Biol. 17*, 463-516.
15. Karadag, A., Fedarko, N. S., and Fisher, L. W. (2005) Dentin matrix protein 1 enhances invasion potential of colon cancer cells by bridging matrix metalloproteinase-9 to integrins and CD44, *Cancer Res. 65*, 11545-11552.
16. Desai, B., Rogers, M. J., and Chellaiah, M. A. (2007) Mechanisms of osteopontin and CD44 as metastatic principles in prostate cancer cells, *Mol. Cancer 6*, 18-42.
17. Redondo-Munoz, J., Ugarte-Berzal, E., Terol, M. J., Van den Steen, P. E., Hernandez del Cerro, M., Roderfeld, M., Roeb, E., Opdenakker, G., Garcia-Marco, J. A., and Garcia-Pardo, A. (2010) Matrix metalloproteinase-9 promotes chronic lymphocytic leukemia b cell survival through its hemopexin domain, *Cancer Cell 17*, 160-172.
18. Redondo-Munoz, J., Ugarte-Berzal, E., Garcia-Marco, J. A., del Cerro, M. H., Van den Steen, P. E., Opdenakker, G., Terol, M. J., and Garcia-Pardo, A. (2008) Alpha4beta1 integrin and 190-kDa CD44v constitute a cell surface docking complex for gelatinase B/MMP-9 in chronic leukemic but not in normal B cells, *Blood 112*, 169-178.
19. Stefanidakis, M., Bjorklund, M., Ihanus, E., Gahmberg, C. G., and Koivunen, E. (2003) Identification of a negatively charged peptide motif within the catalytic domain of

progelatinases that mediates binding to leukocyte beta 2 integrins, *J. Biol. Chem. 278*, 34674-34684.

20. Bjorklund, M., Heikkila, P., and Koivunen, E. (2004) Peptide inhibition of catalytic and noncatalytic activities of matrix metalloproteinase-9 blocks tumor cell migration and invasion, *J. Biol. Chem. 279*, 29589-29597.
21. Ugarte-Berzal, E., Bailon, E., Amigo-Jimenez, I., Vituri, C. L., del Cerro, M. H., Terol, M. J., Albar, J. P., Rivas, G., Garcia-Marco, J. A., and Garcia-Pardo, A. (2012) A 17-residue sequence from the matrix metalloproteinase-9 (MMP-9) hemopexin domain binds alpha4beta1 integrin and inhibits MMP-9-induced functions in chronic lymphocytic leukemia B cells, *J. Biol. Chem. 287*, 27601-27613.
22. Ugarte-Berzal, E., Bailon, E., Amigo-Jimenez, I., Albar, J. P., Garcia-Marco, J. A., and Garcia-Pardo, A. (2014) A novel CD44-binding peptide from the pro-matrix metalloproteinase-9 hemopexin domain impairs adhesion and migration of chronic lymphocytic leukemia (CLL) cells, *J. Biol. Chem. 289*, 15340-15349.
23. Humphries, M. J., Komoriya, A., Akiyama, S. K., Olden, K., and Yamada, K. M. (1987) Identification of two distinct regions of the type III connecting segment of human plasma fibronectin that promote cell type-specific adhesion, *J. Biol. Chem. 262*, 6886-6892.
24. Garcia-Pardo, A., Wayner, E. A., Carter, W. G., and Ferreira, O. C., Jr. (1990) Human B lymphocytes define an alternative mechanism of adhesion to fibronectin. The interaction of the alpha 4 beta 1 integrin with the LHGPEILDVPST sequence of the type III connecting segment is sufficient to promote cell attachment, *J. Immunol. 144*, 3361-3366.
25. Wayner, E. A., and Kovach, N. L. (1992) Activation-dependent recognition by hematopoietic cells of the LDV sequence in the V region of fibronectin, *J. Cell Biol. 116*, 489-497.
26. Moyano, J. V., Carnemolla, B., Dominguez-Jimenez, C., Garcia-Gila, M., Albar, J. P., Sanchez-Aparicio, P., Leprini, A., Querze, G., Zardi, L., and Garcia-Pardo, A. (1997) Fibronectin type III5 repeat contains a novel cell adhesion sequence, KLDAPT, which binds activated alpha4beta1 and alpha4beta7 integrins, *J. Biol. Chem. 272*, 24832-24836.
27. Dufour, A., Sampson, N. S., Li, J., Kuscu, C., Rizzo, R. C., Deleon, J. L., Zhi, J., Jaber, N., Liu, E., Zucker, S., and Cao, J. (2011) Small-molecule anticancer compounds selectively target the hemopexin domain of matrix metalloproteinase-9, *Cancer Res. 71*, 4977-4988.
28. Birkedal-Hansen, H., Moore, W. G., Bodden, M. K., Windsor, L. J., Birkedal-Hansen, B., DeCarlo, A., and Engler, J. A. (1993) Matrix metalloproteinases: a review, *Crit. Rev. Oral Biol. Med. 4*, 197-250.
29. Nagase, H., Suzuki, K., Morodomi, T., Enghild, J. J., and Salvesen, G. (1992) Activation mechanisms of the precursors of matrix metalloproteinases 1, 2 and 3, *Matrix Suppl. 1*, 237-244.
30. Galazka, G., Windsor, L. J., Birkedal-Hansen, H., and Engler, J. A. (1996) APMA (4-aminophenylmercuric acetate) activation of stromelysin-1 involves protein interactions in addition to those with cysteine-75 in the propeptide, *Biochemistry 35*, 11221-11227.
31. Belmokhtar, C. A., Hillion, J., and Segal-Bendirdjian, E. (2001) Staurosporine induces apoptosis through both caspase-dependent and caspase-independent mechanisms, *Oncogene 20*, 3354-3362.
32. Lu, P., Takai, K., Weaver, V. M., and Werb, Z. (2011) Extracellular matrix degradation and remodeling in development and disease, *Cold Spring Harb. Perspect. Biol. 3*, 1-25
33. Bonnans, C., Chou, J., and Werb, Z. (2014) Remodelling the extracellular matrix in development and disease, *Nat. Rev. Mol. Cell Biol. 15*, 786-801.
34. Radisky, E. S., Sarmazdeh, M. R., and Radisky, D. C. (2017) Therapeutic Potential of Matrix Metalloproteinase Inhibition in Breast Cancer, *J. Cell Biochem. 118*, 3531-3548

35. Wojtowicz-Praga, S. M., Dickson, R. B., and Hawkins, M. J. (1997) Matrix metalloproteinase inhibitors, *Invest. New Drugs 15*, 61-75.
36. Palacios, E. H., and Weiss, A. (2004) Function of the Src-family kinases, Lck and Fyn, in T-cell development and activation, *Oncogene 23*, 7990-8000.
37. Hsia, D. A., Lim, S. T., Bernard-Trifilo, J. A., Mitra, S. K., Tanaka, S., den Hertog, J., Streblow, D. N., Ilic, D., Ginsberg, M. H., and Schlaepfer, D. D. (2005) Integrin alpha4beta1 promotes focal adhesion kinase-independent cell motility via alpha4 cytoplasmic domain-specific activation of c-Src, *Mol. Cell Biol. 25*, 9700-9712.
38. Li, L., Okura, M., and Imamoto, A. (2002) Focal adhesions require catalytic activity of Src family kinases to mediate integrin-matrix adhesion, *Mol. Cell Biol. 22*, 1203-1217.
39. Zhao, X. K., Cheng, Y., Liang Cheng, M., Yu, L., Mu, M., Li, H., Liu, Y., Zhang, B., Yao, Y., Guo, H., Wang, R., and Zhang, Q. (2016) Focal Adhesion Kinase Regulates Fibroblast Migration via Integrin beta-1 and Plays a Central Role in Fibrosis, *Sci. Rep. 6*, 19276-19288.
40. Westhoff, M. A., Serrels, B., Fincham, V. J., Frame, M. C., and Carragher, N. O. (2004) SRC-mediated phosphorylation of focal adhesion kinase couples actin and adhesion dynamics to survival signaling, *Mol. Cell Biol. 24*, 8113-8133.
41. Brown, M. C., Cary, L. A., Jamieson, J. S., Cooper, J. A., and Turner, C. E. (2005) Src and FAK kinases cooperate to phosphorylate paxillin kinase linker, stimulate its focal adhesion localization, and regulate cell spreading and protrusiveness, *Mol. Biol. Cell 16*, 4316-4328.
42. Mitra, S. K., and Schlaepfer, D. D. (2006) Integrin-regulated FAK-Src signaling in normal and cancer cells, *Curr. Opin. Cell Biol. 18*, 516-523.
43. Wu, L., Bernard-Trifilo, J. A., Lim, Y., Lim, S. T., Mitra, S. K., Uryu, S., Chen, M., Pallen, C. J., Cheung, N. K., Mikolon, D., Mielgo, A., Stupack, D. G., and Schlaepfer, D. D. (2008) Distinct FAK-Src activation events promote alpha5beta1 and alpha4beta1 integrin-stimulated neuroblastoma cell motility, *Oncogene 27*, 1439-1448.
44. Sen, B., and Johnson, F. M. (2011) Regulation of SRC family kinases in human cancers, *J. Signal Transduct. 2011*, 865819-865833.
45. Osherov, N., and Levitzki, A. (1994) Epidermal-growth-factor-dependent activation of the src-family kinases, *Eur. J. Biochem. 225*, 1047-1053.
46. Mao, W., Irby, R., Coppola, D., Fu, L., Wloch, M., Turner, J., Yu, H., Garcia, R., Jove, R., and Yeatman, T. J. (1997) Activation of c-Src by receptor tyrosine kinases in human colon cancer cells with high metastatic potential, *Oncogene 15*, 3083-3090.
47. Vandooren, J., Born, B., Solomonov, I., Zajac, E., Saldova, R., Senske, M., Ugarte-Berzal, E., Martens, E., Van den Steen, P. E., Van Damme, J., Garcia-Pardo, A., Froeyen, M., Deryugina, E. I., Quigley, J. P., Moestrup, S. K., Rudd, P. M., Sagi, I., and Opdenakker, G. (2015) Circular trimers of gelatinase B/matrix metalloproteinase-9 constitute a distinct population of functional enzyme molecules differentially regulated by tissue inhibitor of metalloproteinases-1, *Biochem. J. 465*, 259-270.
48. Yu, X., Miyamoto, S., and Mekada, E. (2000) Integrin alpha 2 beta 1-dependent EGF receptor activation at cell-cell contact sites, *J. Cell Sci. 113 (Pt 12)*, 2139-2147.
49. Friedl, P., and Wolf, K. (2003) Tumour-cell invasion and migration: diversity and escape mechanisms, *Nat. Rev. Cancer 3*, 362-374.
50. Alford, V. M., Roth, E., Zhang, Q., and Cao, J. (2016) A Novel Collagen Dot Assay for Monitoring Cancer Cell Migration, *Methods Mol. Biol. 1406*, 181-187.
51. Knight, C. G., Willenbrock, F., and Murphy, G. (1992) A novel coumarin-labelled peptide for sensitive continuous assays of the matrix metalloproteinases, *FEBS Lett. 296*, 263-266.
52. Mosmann, T. (1983) Rapid colorimetric assay for cellular growth and survival: application to proliferation and cytotoxicity assays, *J. Immunol. Methods 65*, 55-63.

53. Deryugina, E. I., and Quigley, J. P. (2008) Chick embryo chorioallantoic membrane model systems to study and visualize human tumor cell metastasis, *Histochem. Cell Biol. 130*, 1119-1130.
54. Ribatti, D., Nico, B., Vacca, A., Roncali, L., Burri, P. H., and Djonov, V. (2001) Chorioallantoic membrane capillary bed: a useful target for studying angiogenesis and anti-angiogenesis in vivo, *Anat. Rec. 264*, 317-324.
55. Ribatti, D., Nico, B., Vacca, A., and Presta, M. (2006) The gelatin sponge-chorioallantoic membrane assay, *Nat. Protoc. 1*, 85-91.
56. LeBleu, V. S., Macdonald, B., and Kalluri, R. (2007) Structure and function of basement membranes, *Exp. Biol. Med. (Maywood) 232*, 1121-1129.
57. Imai, K., and Okada, Y. (2008) Purification of matrix metalloproteinases by column chromatography, *Nat. Protoc. 3*, 1111-1124.

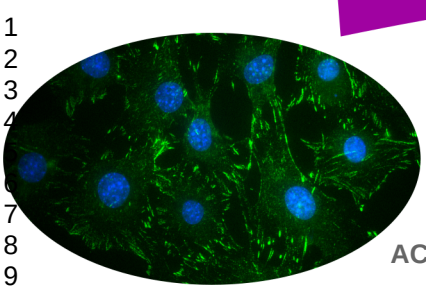

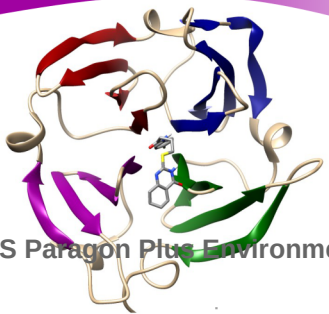

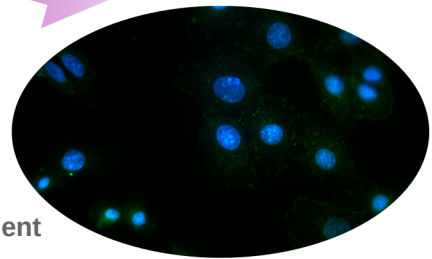

cell migration and invasion

blocked metastasis